MULTI YEAR AEROSOL CHARACTERIZATIONIN THE TROPICAL ANDES AND IN ADJACENT AMAZONIA USING AERONET MEASUREMENTS

Daniel Pérez-Ramírez[1,2], Marcos Andrade[3],Tom Eck[4,5],Ariel Stein[6],Norm O'Neill[7], Hassan Lyamani[1,2], Santiago Gassó[8,9], David N. Whiteman[10], Igor Veselovskii[11,12], Fernando Velarde[3]and Alados-Arboledas, L.[1,2]

[1]Applied Physics Department, University of Granada, 18071,Granada, Spain

[2]Andalusian Institute for Earth System Research (IISTA), Av.Mediterráneo s/n, 18006, Granada, Spain

[3]LaboratoryforAtmosphericPhysics, Universidad Mayor de San Andrés, La Paz, Bolivia.

[4]Goddard Earth Sciences Technology and Research, University Space Research Association (GESTAR/USRA), 21040, Columbia, Maryland, United States·

[5]Biospheric Sciences Laboratory, NASA Goddard Space Flight Center, 20771, Greenbelt, Maryland, United States.

[6]NOAA Air Resources Laboratory, 5830 University Research Court, 20740, College Park, Maryland, United States

[7]Centre d'Applications et de Recherches en Telédetection, Université de Sherbrooke, Sherbrooke, Canada

[8]Morgan State University, Maryland, United States

[9]Climate and Radiation Laboratory, NASA Goddard Space Flight Center, 20771, Greenbelt, Maryland, United States.

[10]Mesoscale Atmospheric Processes Laboratory, NASA Goddard Space Flight Center, 20771, Greenbelt, Maryland, United States.

[11]Joint Center for Earth Systems Technology, University of Maryland Baltimore County, Baltimore, Maryland, United States.

[12]Physics Instrumentation Center of General Physics Institute, Troitsk, Moscow, Russia

Correspondence to: Daniel Perez-Ramirez; E-mail: dperez@ugr.es;

ABSTRACT

This work focuses on the analysis of columnar aerosol properties in the complex geophysical tropical region of South America within 10-20° South and 50-70° West. The region is quite varied and encompasses a significant part of Amazonia (lowlands) as well as high mountains in the Andes (highlands,~4000 m a.s.l.). Several AERONET stations were included to study the aerosol optical characteristics of the lowlands (Rio Branco, Ji Parana and Cuiaba in Brazil and Santa Cruz in Bolivia) and the highlands (La Paz, Bolivia) during the 2000-2014 period. Biomass-burning is by far the most important source of aerosol in the lowlands, particularly during the dry season (August-October). Multi-annual variability was investigated and showed very strong burning activity in 2005, 2006, 2007 and 2010. This resulted in smoke characterized by correspondingly strong, above-average AODs (aerosol optical depths) and homogeneous single scattering albedo (SSA) across all the stations (~0.93). For other years, however, SSA differences arise between the northern stations (Rio Branco and Ji Parana) with SSAs of ~0.95 and the southern stations (Cuiaba and Santa Cruz) with lower SSAs of ~0.85. Such differences are explained by the different types of vegetation burned in the two different regions. In the highlands, however, the transport of biomass burning smoke is found to be sporadic in nature. This sporadicity results in highly variable indicators of aerosol load and type (Angstrom exponent and fine mode fraction) with moderately significant increases in both. Regional dust and local pollution are the background aerosol in this highland region, whose elevation places it close to the free troposphere. Transported smoke particles were generally found to be more optical absorbing than in the lowlands: the hypothesis to explain this is the significantly higher amount of water vapor in Amazonia relative to the high mountain areas. The air-mass transport to La Paz was investigated using the HYSPLIT air-concentration five-days

back trajectories. Two different patterns were clearly differentiated: westerly winds from the Pacific that clean the atmosphere and easterly winds favoring the transport of particles from Amazonia.

1.- Introduction

High mountain areas are very sensitive to climate change as they host many glaciers and are also involved in many cloud formation processes (e.g. Wonsick et al., 2014; Lüthi et al., 2015). Particularly, high mountains in tropical areas are the host of glaciers and snow at such latitudes, irrigating many rivers and thus are essential for the water supply of local population. Changes in glacial and snow covers are indicators of climate change (e.g. Xu et al., 2016). The Andes in South America is the largest mountain chain in the world covering a latitude range from -55º S to 5ºN and with many peaks above 5000 m a.s.l. The Andes mountain chain is part of many countries and is a natural barrier between the bulk of the South American mainland and the Pacific Ocean. It also represents a fundamental constraint on the eastern meteorology given the predominance of easterly trade winds from the Atlantic Ocean. These trade winds create the conditions for the South American Low Level Jet (SALLJ) that runs parallel to the mountains (Ulke et al., 2011). The SALLJ exhibits an annual cycle that peaks during austral summer and is the major air-mass transport mechanism in South America. Despite its low altitude (around 1500 m a.s.l.), it enhances moisture availability for convection in the Andes Mountains (Nogués-Paegle and Mo, 1997).In other regions containing large mountain chains such as the Himalaya in Asia or the Alps in Europe many studies have been done concerning trace gases (e.g. Schwikowski et al., 1999; Maione et al., 2011), aerosols (e.g. Gautman et al., 2011; Zieger et al.,

2012) and cloud formation (e.g. Bonasoni et al., 2010). In the Andes, however, due to the lack of appropriate measurements, these topics have not been studied well.

The Amazon Basin is a major source of anthropogenic-driven biomass-burning emissions (e.g. Mishra et al., 2015), accounting for approximately 15% of total global biomass-burning emissions (van der Werfet al., 2010).Depending on the vegetation burned, fires inject reactive gases, greenhouses gases (e.g. as carbon dioxide (CO_2) and methane (CH_4)) and particles into the atmosphere (Andreae and Merlet, 2001; Bowman et al., 2009; Remy et al., 2014).Biomass-burning emissions are also a major source of organic (14-77 Tg/yr) and black carbon particles (1.8-11 Tg/yr)(e.g. Bond et al., 2013). Aerosol smoke particles that are the result of biomass-burning directly affect the Earth-Atmosphere radiative budget by scattering and absorbing solar radiation (e.g. Jacobson, 2014) and also indirectly by acting as cloud condensation nuclei (CCN) and ice nuclei (IC) and thereby changing the distribution and properties of clouds (e.g. Koren et al., 2008). Biomass-burning can be the cause of serious public health issues such as extreme particulate matter (PM) concentrations caused by fires in the island of Borneo and Sumatra (Eck et al., 2016). Smoke from wildfires has also been associated with both increased mortality (Vedal and Dutton, 2006) and morbidity (Bowman and Johnston, 2005), and may cause ~250,000 (73,000–435,000) premature mortalities/yr, with >90% being associated with PM (Jacobson, 2014).

In Amazonia the smoke emissions caused by agricultural burning of residues (e.g. Uriarte et al., 2009) and by deforestation along the borders of Amazon forests, known as the arc of deforestation (e.g. Morton et al., 2008; van Marle et al., 2016). The burned areas are commonly found in Brazil, Peru, Colombia, Bolivia, Paraguay and northern Argentina. Atmospheric transport patterns lead to spatial distributions of smoke that can be very different from the

distribution of the actual fire sources (e.g. Freitas et al., 2005). This, in turn, has differing impacts on different environments and populations. As an example, many studies have been carried out over Brazilian areas, including modeling transport efforts (e.g. Matichuk et al., 2008; Longo et al., 2010) and the impact of smoke over both rural areas and highly populated cities (e.g. Reid et al., 1998,1999; Kotchenruther et al., 1998). Also, intensive field campaigns such as GOAMAZON (http://campaign.arm.gov/goamazon2014/) have been staged to advance the understanding of absorption and aging properties of smoke, of greenhouse gases and of smoke transport patterns. However, due to the enormous areas burned and the population differences as well as different agricultural traditions and agricultural development between Brazil and its neighbors, the study of biomass burning in the rest of South America needs to be the focus of more investigations.

The main objective of this work is to analyze the smoke particle patterns in the Bolivian Andes and surrounding areas. To that end, we focus on the long-term ground-based measurements of the AERONET network acquired at the high mountain site in the city of La Paz (3340 m a.s.l) and at nearby lowland sites in Brazil and Bolivia.We usedthe HYSPLIT model (Stein et al., 2015) to interpret the origin of the air masses influencing the study region. Biomass-burning smoke studies using AERONET data have been successfully carried out in Brazil (e.g. Schafer et al., 2008), Africa (e.g. Eck et al., 2003, 2013: Queface et al., 2011) and in Alaska (e.g. Eck et al., 2009) as well as for cases of long-range transport of biomass burning smoke in North America (e.g. Colarco et al., 2003; Veselovskii et al., 2015), Europe (e.g. Alados-Arboledas et al., 2011) and Asia (e.g. Noh et al., 2009). AERONET data on biomass-burning smoke have also been used to improve and validate satellite retrievals (e.g. Sayer et al., 2014).

125 This work is structured as follows: Section II describes the experimental region and
126 methodology. The results are in Section III and concluding remarks in section IV.

127 2.- Experimental Region and Methodology

128 The South American study zone of interest is in the tropical region within 10-20° South
129 and 50-70° West. The area includes three different geophysical regions: The Amazon (lowlands)
130 is characterized by tropical conditions, the high mountain regions by mountains above 6000 m
131 a.s.l. that also include flat areas known as the 'Altiplano' (highlands ~ 4000 m a.s.l.) and by a
132 transition between the two (foothills). Figure 1 shows a map of the area, including the
133 AERONET stations whose data were used in this study and an example of an elevation profile
134 from the Pacific Ocean to Amazonia crossing the La Paz region. The wet season occurs during
135 the period from December to March, and the dry season is particularly intense in the period from
136 June to September. The most important geo-atmospheric factor is the strong altitude gradient
137 between the lowlands and highlands, with its attendant large differences in water vapor content
138 and relative humidity. The city of La Paz, Bolivia (16.36º South, 68.06º West, 3439 m a.s.l.),
139 which is located in a valley surrounded by mountains of up to 5500 m a.s.l is an important focus
140 of this study. The metropolitan area includes the Andean Altiplano with a total population of
141 around 1.7 million inhabitants. The lowlands to the north and east include the stations of Rio
142 Branco, Brazil (9.95º South, 67.87º West, 212 m a.s.l.), Cuiaba, Brazil (15.50º South, 56.00º
143 West, 250 m a.s.l.) and Ji-Parana, Brazil (10.85º South, 61.80º West, 100 m a.s.l.) These stations
144 are close to small-medium sized cities with populations in the range of 120,000-600,000
145 inhabitants. The station in the Bolivian city of Santa Cruz de la Sierra (17.08º South, 63.17º
146 West, 442 m a.s.l.) with a total population of 2 million was also included in our study.

147 Anthropogenic aerosol emissions from these cities, particularly road traffic emissions, are the
148 main sources of local anthropogenic aerosol over the study region.

149 Column-integrated characterization of atmospheric aerosol was examined using
150 AERONET sun-photometry measurements. The standard AERONET instrument is the well-
151 knownCIMEL CE-318-4 sun photometer. This device measures direct sun signals at 340, 380,
152 440, 500, 675, 870, and 1020 nm which are transformed into aerosol optical depths (AODs).
153 Details of AERONET sun photometers including calibration, error analysis and aerosol optical
154 properties retrievals are in Holben et al., (1998), Eck et al.,(1999) and in Smirnov et al., (2000).
155 All the data used in this study are cloud-screened and quality assured (Level 2.0).

156 Within the solar spectrum, the Angström exponent is a good indicator of the predominant
157 size of atmospheric particles (i.e. Dubovik et al., 2002): $\alpha > 1.5$ implies the predominance of
158 fine mode (submicron) aerosols while $\alpha < 0.5$ implies the predominance of coarse mode
159 (supermicron) aerosols. However, for a more accurate characterization of the relative influence
160 of fine and coarse mode particles an interpretation based solely on very high or very low values
161 of α is not straightforward. We accordingly used the Spectral Deconvolution Algorithm (SDA)
162 product incorporated into AERONET standardized processing (O'Neill et al., 2001a,b; 2003), to
163 study fine mode AOD (AOD_{fine}), coarse mode AOD (AOD_{coarse}), and fine mode fraction
164 ($\eta = AOD_{fine} / AOD$) at a reference wavelength of 500 nm.

165 In terms of aerosol microphysical properties, the operational AERONET algorithm
166 (Dubovik and King, 2000; Dubovik et al., 2000) uses sky radiances and direct sun measurements
167 as inputs and provides retrieved aerosol size distribution as well as intensive properties such as
168 aerosol refractive index, single scattering albedo (SSA) and asymmetry factor (g) (across four

169 spectral bands at 440, 675, 870, 1020 nm). However, the AERONET algorithm has specific and
170 often difficult to satisfy sky condition requirements (Holben et al., 2006) in that skies must be
171 completely clear and large scattering angles (typically larger than 50º). These limitations imply
172 that refractive index retrievals are only reliable for AOD > 0.4, although not for the retrieval of
173 size distribution (Holben et al., 2006). It accordingly provides low temporal resolution results
174 (generally a maximum of approximately 8 inversions per day are possible). Nevertheless,
175 retrievals that uses sky radiance measurements are the only that are able to provide retrieved
176 values of aerosol refractive index, single scattering albedo and phase function with appropriate
177 accuracy (Dubovik et al., 2006).

178 To complement AERONET retrieved aerosol microphysical properties, we compute
179 additional retrievals using the Linear Estimation technique (Veselovskii et al., 2012, 2013), that
180 uses AERONET spectral AODs measurements as input to yield high frequency estimates of
181 aerosol microphysical parameters during the whole day. The parameters retrieved using the LE
182 technique are the effective radius (r_{eff}) and the volume concentration (V). The other retrievals we
183 ran were based on the method proposed by O´Neill et al., (2005, 2008a), which, itself, is based
184 on the spectral curvature of the fine mode Angstrom slope and its spectral derivative, derived
185 from the SDA. This algorithm is used to estimate the fine mode effective radius (r_{fine}).

186 The inversions by LE are constrained in the maximum radius allowed in the inversion due
187 to the range of AODs used in the inversion (380 - 1020 nm), being improved the retrieval
188 accuracy. Measurements of α(440-870) are used for the selection of the maximum radius in the
189 inversion, being of 2 μm for fine mode predominance and of 10 μm for the rest of cases. Also,
190 simulations revealed that LE retrievals have an accuracy below 20% for r_{fine} > 0.12 μm, while the
191 accuracy degrades for lower r_{fine} due to the lack of sensitivity of the inversion range to these tiny

192 particles. Posterior comparisons versus AERONET retrievals showed differences of up to 10 %
193 for fine mode predominance and 20 % for coarse mode predominance. The largest uncertainties
194 were found for mixtures of both modes with differences up to 30%. Because the use of LE
195 retrievals is for supporting AERONET inversions, corrections functions are applied which
196 reduced the differences between the two retrieval schemes to generally less than 10%. We
197 remark here that AERONET uncertainties are similar to these ranges being (Dubovik et al.,
198 2000). More details about the use of Linear Estimation retrievals are in Perez-Ramirez et al.,
199 (2015). On the other hand, for the retrievals of r_{fine} using O'Neill et al., (2005, 2008a)
200 methodology, comparisons versus AERONET retrievals for the limited data set of O'Neill et al.,
201 2005 and confirmed by more recently unpublished AERONET-wide comparisons show average
202 differences ~ 10% for η values >~ 0.5.

203 The HYSPLIT model (Stein et al., 2015), developed by the NOAA Air Resources
204 Laboratory, and accessible on-line at http://www.ready.noaa.gov/HYSPLIT.php is used to
205 compute air parcel backward-trajectories and from them assess dispersion of aerosols. The
206 meteorological data used to run the model were from 6-hourly GDAS (Global Data Assimilation
207 http://www.emc.ncep.noaa.gov/gmb/gdas/) output at 1° degree horizontal resolution. The total
208 trajectory time was set to 120 hours.

209

210 3.- Results

211 3.1. Aerosol Optical Properties

212 Figure 2 shows the temporal evolution of daily means of AOD, AOD_{fine} and AOD_{coarse} for
213 the AERONET stations, whose data were employed in our study (with a zoomed insert of the

temporal plot of the highlands station of La Paz). The reference wavelength is 500 nm. Table 1 presents a statistical summary of the parameters in Figure 2, particularly mean values, standard deviations (*STD*), medians, maxima and minima.

[Insert Figure 2 here]

[Insert Table 1 here]

Maxima of AOD, AOD_{fine} and AOD_{coarse}occur during the biomass-burning season from August to October. The intensity of the biomass-burning season varies from year to year as evidenced, for example, by the different maximum values of Figure 2. These intense biomass-burning seasons have also been reported in the literature based on satellite observations (e.g. Torres et al., 2010). During the biomass-burning season, increases in AOD_{fine} and AOD_{coarse} are observed when compared with other seasons. But the increase of AOD_{fine} is very large compared to that of AOD_{coarse}, indicating a large predominance of fine particles (by about an order of magnitude).

The differences in the maximum values of AODs among the different biomass-burning seasons imply a multi-year variability in fire emissions, which is consistent with the large standard deviation of AODs reported in Table 1. Emissions of smoke particles from biomass burning are mostly associated with human activities. Examples of this are fires that are used for forest clearing by small farmers and plantation owners who clear understory shrubbery and cut forest trees. The area is burned a few months after the clearing, and, although the fires are intended to only burn in limited areas, they sometimes spread beyond the targeted agricultural zone and consume pristine rainforest (e.g. Torres et al., 2010). The extent and intensity of the burned areas can vary from year to year.

236 To show that the data used are predominately cloud-free, Figure 3 shows α(440-870)
237 versus AOD(500) for lowland stations. Cloud-affected data typically present α(440-870)< 0.5
238 (O´Neill et al., 2003). In particular, AODs > 2 are associated with α(440-870) values that are
239 generally> 1.2, a value which suggests minimal cloud contamination in the measurements.
240 Moreover, the number of photocounts is large enough to guarantee the quality of the
241 measurements: for very high AODs the number of photocounts registered by the AERONET
242 instruments ranged from about 50 to 20 counts for 500 nm AODs of 4 and 6 respectively at the
243 Cuiaba site, while the minimum count required for good AOD measurement is 10 (Sinyuk et al.,
244 2012).
245 The analyses of η is useful for detecting when AOD measurements are affected by thin
246 and stable cirrus clouds (O'Neill et al., 2003). Measurements affected by cirrus clouds present
247 low η because these clouds are formed by big ice crystals. Indeed, for aerosol with fine mode
248 predominance and not affected by cirrus η present high values. This approach can be applied for
249 smoke particles. The analyses performed of η values for Figure 3 data reveal that measurements
250 with AOD > 2.0 (71 days totally) present η > 0.85, suggesting no presence of clouds. For 1 <
251 AOD < 2 were registered 220 days of measurements, and it is found that 94% with η > 0.9, and
252 only 4 days of measurements with η < 0.75 that could be associated with influence of thin cirrus
253 clouds. Finally, for 394 days of measurements that presented 0.5 < AOD < 1, were registered
254 82% of cases with η > 0.9 and 94% with η > 0.8. The rest of the cases with lower η can be
255 associated with aerosol influenced by coarse particles, although the presence of thin cirrus clouds
256 cannot be discarded.

257 [Insert Figure 3 here]

258 The maximum values reported in Figure 2 represent some of the largest values ever
259 registered in the AEROENT Version 2 database (http://aeronet.gsfc.nasa.gov/cgi-
260 bin/climo_menu_v2_new). The mean values during the biomass-burning season are also among
261 the largest monthly mean climatological values. Schafer et al., (2008) registered similar values
262 using stations located in the Amazon basin. Comparably high AOD values were also reported for
263 African biomass-burning by Eck et al., (2003, 2013). Moreover, the occurrence of very high
264 AOD values over the extended periods of time that we have reported here are only obtained in
265 very polluted parts of Asia (e.g. Eck et al., 2010), very dusty areas in the Sahara (e.g. Guirado et
266 al., 2014) and the Arabian Peninsula (e.g. Kim et al., 2011).

267 For the highland La Paz station the AOD increased during the August-October period
268 from mean values around 0.09 to 0.12 (Table 1), but the AOD values are much lower than those
269 in the lowlands. Although the fine mode is still predominant, the contribution of coarse mode to
270 the total AOD cannot be ignored. The frequency histograms of AOD(500) for each station are
271 given in Figure 4, and they show that only 7 % of data at La Paz present AOD > 0.4 while for the
272 stations of Cuiaba, Ji Parana, Rio Branco and Santa Cruz these percentages are of 45%, 59%,
273 44% and 41% respectively. That indicates the greater contribution of biomass-burning particles
274 in the lowlands to the total aerosol load and to the aerosol seasonal changes.

275 Multi-wavelength lidar measurements in the central Amazon made by Baars et al., (2012)
276 showed that smoke plumes can reach altitudes up to 5 km. During the burning season, the
277 reduced vegetation in the highlands implies few fires, while the large AODs in the lowlands
278 suggests that transport of smoke particles from nearby Amazonia is the main source of particles.
279 The Andes chain in the tropics is therefore a barrier for the transport of smoke to the Pacific
280 Ocean, in agreement with the results of Bourgeois et al., (2015) using CALIPSO data.

281 [Insert Figure 4 here]

282 Indicators of particle type predominance between biomass and non-biomass burning
283 seasons is illustrated in Figure 5, where Box-Whisker plots of α(440-870) and fine mode fraction
284 are represented. In the Box-Whisker plots, the mean is represented by a very small open square
285 within a given rectangle. The horizontal line segment in the rectangle is the median. The top
286 limit (top of the rectangle) represents the 75th percentile (*P75*) and the bottom limit the 25th
287 percentile (*P25*). The lines perpendicular to the boxes are the 1st (*P1*) and 99th (*P99*) percentiles,
288 and the crosses represent the maximum and minimum values respectively

289 [Insert Figure 5 here]

290 Figure 5 shows very high values of α(440-870)in the lowlands during the biomass-
291 burning seasons, with mean values of 1.5-1.7 which are similar to biomass-burning values
292 reported in the literature (e.g. Dubovik et al., 2002; Schafer et al. 2008) and, along with the
293 values of η above 0.80, indicate a predominance of fine particles. Lower values of α(440-870),
294 characterized by large standard deviations, are observed for the non-biomass burning seasons.
295 The mean values also vary significantly among stations (from 0.86 at Rio Branco to 1.36 at Santa
296 Cruz). These results, plus the fact that the values of η vary between 0.7 and 0.5, indicate a lack of
297 predominance of fine or coarse mode in the wet season. Indeed, a mixture of different particles
298 predominates. On the other hand, the mean Angstrom Exponent values of 0.94 and 0.85 for the
299 biomass and non-biomass burning seasons, respectively at the highland station of La Paz, are not
300 significantly different after considering the standard deviation. The same is true for η, with mean
301 values of 0.55 and 0.48 respectively. These La Paz values of α(440-870) and η cannot,
302 accordingly, be associated with large predominance of either fine or coarse mode.

303 The multi-year and seasonal variability of AOD and α(440-870) in the highland station is
304 illustrated in Figure 6 as a function of the day of the year. Mean values are represented by dots
305 and standard deviations by vertical lines. These values are the result of averaging AOD for each
306 day of the year in different years. During the biomass-burning season mean AOD at 500 nm is of
307 0.12 ± 0.06, but the standard deviations of the means indicate AOD peaks of up to 0.35, and are
308 typical values associated with the transport of biomass-burning particles to high mountain places
309 (e.g. Perez-Ramirez et al., 2008). For other high mountain sites in the Himalayas during the pre-
310 monsoon season, values of up to 0.1 are reported at elevations of ~ 5000 m a.s.l. (Marcq et a.,
311 2010) and up to 0.5 at elevations of ~ 2000 m a.s.l. (Dumka et al., 2008). Therefore, the values
312 obtained in La Paz station are similar to high-mountain Himalayan sites affected by the transport
313 of pollutants. The large standard deviations of AODs in the biomass-burning season also indicate
314 large variability, which suggests that the arrival of smoke particles occurs during sporadic events
315 rather than as part of a continuous. AODs values during the other seasons (especially in the
316 April-July period), are ~ 0.1 and are considered as background conditions (local
317 origins).Therefore, biomass-burning transport to high mountains can induce AOD values of up to
318 five times the average background conditions. In section 3.4, we study several such events in
319 detail. The period November-March (wet season) exhibits large variability, which might be
320 explained by meteorological factors such as wet deposition and by the less robust statistics of the
321 smaller database associated with that period.

322 [Insert Figure 6 here]

323 The parameter α(440-870) shows mean values that are not significantly different during
324 the biomass burning season as compared with the other seasons (Figure 6b). This suggests that
325 the particle type predominance during the biomass-burning season is similar to that in other

seasons (which are probably dominated by aerosols of local origin). Actually, during the biomass-burning season, mean α(440-870) values are around 1.0 while values for background conditions (focussing on the April-July period with mean AODs of ~0.09) α(440-870) are around 0.85. In the wet season (November-March), the larger variability observed in Figure 6 can be explained by the low AODs (<0.05) which implies larger uncertainties in α(440-870).

The frequency of sporadic smoke events transported to La Paz can be observed in the α(440-870) versus AOD graph of Figure 7 (whose dataset is limited to the biomass-burning season).In order to discriminate AOD contributions associated with thetransport of smoke from background AODs, we established AOD > 0.14, which is the mean plus standard deviation value during the non biomass-burning season (Table 1), as a criterion for classifying intense smoke events. Analyses of Figure 7 data indicate that only 10 % of the measurements acquired during the biomass-burning season exceed this threshold. The cases of smoke transport are characterized by a considerably higher α(440-870) (1.4 ± 0.2) versus the background. Since there is no other extra source than episodic biomass-burning aerosols (emissions by local sources are almost constant throughout the year), the large differences in the Angstrom exponent associated with smoke between lowlands (~1.8) and highlands (~1.4) suggest changes in smoke particles during their transport to the highlands. This could also suggest a larger influence of local coarse mode particles at La Paz since the maximum AOD values are much lower there than in the Amazonian Basin.

[Insert Figure 7 here]

3.2. Biomass-burning and precipitation rates

Table 2 reports the rainfall difference between values registered and climatological values for each season. Such difference is defined here as rainfall anomaly. Data used are from

TRMM satellite (http://trmm.gsfc.nasa.gov) for the period 2002-2014 in the study area (10-20º South, 50-70º West.). The mean of the TRMM data are taken as the climatological values and are shown in parentheses. The 'wet' period was taken to be November-March, the 'dry' period to be April-July while the biomass burning period was taken as August-October.

[Insert Table 2 here]

An anomalous precipitation increase during the wet period can increase the amount of vegetation to be burned during the biomass-burning season (Uhl et al., 1998). Increases in precipitation during the biomass-burning period favors particle wet deposition and the shortening of aerosol lifetimes (Freitas et al., 2005). An increase in aerosol loads can be expected for the dry and biomass burning periods due to unusually dry conditions that intensify fire activity. Such links with precipitation seem to be clear for the intense biomass-burning activity (as represented by AOD amplitude in Figure 2) registered in 2005-2010: positive rainfall anomalies in the wet season could have increased the amount of biomass that could be burned in the following burning season, while negative rainfall anomalies in the dry and / or burning seasons could have favored fire activity. An exception to this pattern is 2009, which exhibits positive rainfall anomalies during the dry and biomass-burning seasons and therefore lowers AODs. However, in 2008 a strange behavior was observed in that dry conditions were present but lower AOD values were recorded compared with 2005, 2006, 2007 and 2010. The strange behavior in 2008 was also reported by Torres et al., (2010) using OMI space-borne sensor data.

The 2002-2004 period (except for the dry period of 2004) exhibits an opposite pattern, with a precipitation deficit in the wet season and positive rainfall anomalies in the dry and burning seasons. The lower AODs for these years are broadly coherent with the concepts presented above on the relationship between rainfall anomaly and fire activity. However, after

2011 the type of reasoning that we have employed above to make the link between rainfall anomaly and fire activity is not followed, as a continuous reduction of AODs and fire activity has been observed independently of precipitation. Specific regulations and/or economic forces as suggested by Koren et al., (2007, 2009) could have helped to reduce fire activity. More years of data and perhaps different level of correlation analyses have to be investigated.

3.2. Aerosol Particle Sizes

Figure 8 shows the mean particle volume size distributions from AERONET almucantar retrievals for the study stations, separated into biomass and non-biomass burning seasons. Different scales are used in the Y-axes between both seasons to better visualize size distribution shapes. This figure indicates that during the biomass-burning season the fine mode largely predominates for the lowland stations. Very similar size distributions for biomass-burning have been reported in the literature (e.g. Eck et al., 2003; Schafer et al., 2008). However, in the highlands the size distribution exhibits two modes with approximately the same volumetric relevance, although that does not imply that both modes have the same optical effect (in the visible spectral range, for the same volume, AOD_{fine} is larger than AOD_{coarse}). This is broadly consistent with the previous results of the $\alpha(440\text{-}870)$ and η analysis: the coarse mode could be associated with the injection of dust particles from the Andean Altiplano, either by traffic re-suspension or regional winds: On-going studies with in-situ instrumentation are revealing that 50 % of PM10 particles are associated with mineral dust (Alastuey et al., 2017). Fine mode particles are likely associated with anthropogenic activity (e.g. vehicle emissions) and with the transport of smoke particles. On the other hand, during the non-biomass burning season, the maxima of volume size distributions are lower in accordance with the lower AODs. It is also observed for all the stations that no mode predominates, but rather, there is an apparent mixture of different

types of particles. This result is also consistent with the intermediate values of α(440-870) and η noted above. For La Paz, the two modes are explained by the same mechanism noted for the biomass-burning case, although the fine mode volume is smaller due to the absence of transported smoke particles.

[Insert Figure 8 here]

The stations in the lowlands, Santa Cruz and Cuiaba show a relevant coarse mode, which is present in both seasons. This coarse mode can be associated with different local sources of dust. Transport of dust from river beds is a possible explanation, as is illustrated in Figure 9 which shows a true color image for the lowland area on 12th September 2016. The image is composed by the different images acquired by MODIS (Aqua and Terra) and VIIRS space systems (images available at http://go.nasa.gov/2eULwP1). The low level jet which runs parallel to the mountain with southerly direction is observed from the clouds and smoke transport patterns. Making a zoom on the river areas, transported dust plumes are observed. Injections of dust from riverbeds have been also observed in Alaska (Crusius et al., 2011). In South America, other regions that could be responsible for transport of dust to the lowlands is the Chaco plain that spreads to the Andes foothills through Bolivia, Argentina and Paraguay, and include some of the largest tributary rivers and delta rivers in the world (Latrubesse et al., 2012). From more southern locations, injections of salt particles in the atmosphere have been observed from the Mar Chiquita Lake (Bucher and Stein, 2016). The Andean region has other possible sources of dust particles such as the Salar de Uyuni or the Atacama Desert (Gaiero et al., 2013). The high latitudes of these two places could have more influence on the injection of particles in the lowlands. Nevertheless, more analysis is needed to study the impact and properties of dust particles in the tropical region of South America.

418 [Insert Figure 9 here]

419 Measurements of water vapor mixing ratio, *w*, derived from different meteorological
420 stations in Bolivia are available for more than 10 years, both for the lowlands and the highlands.
421 For the wet period (November-March) when most precipitation occurs, the highest values of
422 *w*are found (around 19 g/Kg and 8 g/Kg for the lowlands and highlands, respectively). For the
423 dry period (April-July) with very little precipitation the lowest values are found (around 14 g/Kg
424 and 4 g/Kg for the lowlands and highlands, respectively). However, for the biomass-burning
425 season values are in the middle (around 16.5 g/Kg and 5.5 g/Kg for the lowlands and highlands,
426 respectively) indicating the presence of enough water vapor in the atmosphere to favor cloud
427 development which therefore, reduces the number of measurements that fulfil the completely
428 cloud-free sky AERONET criteria for retrieving aerosol microphysical properties. Therefore, due
429 to AODs measurements only require direct sun measurements, LE retrievals and O´Neill et al.,
430 (2005) methodology are used to obtain r_{eff} and r_{fine}, respectively, and complement AERONET
431 retrievals. Actually, during all of the biomass-burning seasons, the number of Level 2.0 retrievals
432 obtained using the almucantar retrieval was 738, 750, 1017, 262 and 206 for the Rio Branco, Ji
433 Parana, Cuiaba, Santa Cruz and La Paz stations, respectively. The number of higher temporal
434 resolution (spectral) retrievals using the LE technique were respectively 16189, 6343, 25017,
435 6719 and 18220 – this is a significant increase in the number of retrievals for the La Paz station
436 compared with the AERONET almucantar retrievals.

437 To understand the spatial differences in retrieved particle radii, station by station, Box-
438 Whisker plots of r_{eff} and r_{fine}, separated into biomass-burning and non biomass-burning seasons,
439 are shown in Figure 10. Table 3 summarizes the main statistical parameters of these plots. Linear
440 Estimation and O'Neill et al., (2005) retrievals are used. Similar patterns and statistics were

441 obtained using only AERONET retrieval data, although less robust statistically. During the
442 biomass-burning season the similarity of the mean values and the low standard deviations of both
443 parameters in the lowlands is remarkable: both of these comparisons indicate an approximate
444 homogeneity in the biomass-burning process with respect to particle size. The relatively large
445 variability in the non biomass-burning season can be explained by the highly variable
446 background aerosol conditions with mixtures of different aerosol types prevailing. The typically
447 larger uncertainties in r_{eff} and r_{fine} for low aerosol loads can also explain some of the increased
448 variability. The Santa Cruz station shows larger r_{eff} during the non biomass-burning season
449 which, as noted before, could be associated with coarse particles transported from local riverbeds
450 as described in association with Figure 9.

451 The highlands show systematically larger values of r_{eff} and r_{fine} independently of the
452 season. The slightly lower values of both parameters during the biomass-burning season can be
453 explained by the transport of smoke particles which, as previously noted, are predominantly fine
454 mode. Aging of the transported particles (e.g. Eck et al., 2003; O'Neill et al., 2008b) could
455 explain the larger r_{eff} and r_{fine}. The permanent coarse mode associated with dust on the Altiplano
456 could also have an influence in terms of an increase in r_{eff}. The wind regime in the high
457 mountains can favour accumulation of particles and can explain the larger values of r_{fine}
458 compared to the lowlands (Vuille, 1999).

459 [Insert Figure 10 here]

460 [Insert Table 3 here]

461 The dependences of particle size on aerosol load is illustrated in Figure 11 where we
462 represent r_{eff} and r_{fine} versus the AOD at 500 nm for the combination of all lowland data. Again,

463 Linear Estimation and O'Neill et al., (2005) are used for the retrievals of r_{eff} and r_{fine},
464 respectively. We constrained the data plotted to conditions of AOD > 1.0 in order to limit the
465 study to smoke particles only. Higher temporal-resolution retrievals of r_{eff} and r_{fine} because do
466 provide larger datasets and also do allow retrievals for very high AODs which and may well be
467 favoured in the case of partly cloudy skies (see our argument above for the greater probability of
468 clouds being associated with smoke aerosols): for example, values of AOD up to 6.0 were
469 measured and the retrievals of linear estimation and O'Neill et al., (2005) were possible, while
470 the almucantar retrievals were limited to measured AODs up to 3.2.

471 [Insert Figure 11 here]

472 Figure 11shows linear trends of r_{eff} and r_{fine} with AOD increases. Similar patterns were
473 obtained by using the operational AERONET almucantar retrieval algorithm, although the lower
474 number of data introduced more uncertainty in the linear regressions. Actually, maximum AODs
475 for AERONET retrievals were for ~3.2, while for data of Figure 11 that maximum is for ~6.0.
476 Root-mean-square differences are ~0.027 for r_{eff} and ~0.016 for r_{fine}. The results of the linear fits
477 shown in Figure 11 indicate that r_{fine} is nominally more sensitive to changes in AOD (the slope of
478 the regression line is larger). The difference, for example, between the minimum and maximum
479 AOD values of 1.0 and 6.0 is 0.035 µm for the associated r_{eff} regression line. This is small
480 compared with the r_{eff} values. The analogous r_{fine} calculation (a regression line increase of 0.065
481 µm for the same range of AODs),corresponds to a change of approximately 40%. Such large
482 aerosol loads favour the accumulation of particles in the atmosphere and, can therefore favor
483 particle aging. For example, larger r_{fine} and r_{eff} have been found during the night due mainly to
484 particle accumulations (e.g. Pérez-Ramírez et al., 2012). Also, coagulation rates increase as
485 particle concentration (or AOD) increases (Colarco et al., 2003). The observed trend of

increasing fine mode particle size in Amazonia as AOD increases is consistent with the findings of Schafer et al. (2008) from AERONET almucantar retrievals.

3.3. Aerosol Single Scattering Albedo, Refractive Index and Asymmetry Factor

For primary (directly retrieved) optical parameters such as the refractive index and derived optical parameters such as the single scattering albedo (SSA) the only source of information in this study is the AERONET almucantar scan/extinction spectrum retrieval. Level 2.0 data, the most reliable inversion product, is constrained by several quality control criteria(see Holben et al., 2006 for more details on the Level 2.0, Version 2.0 inversion criteria). Also, for intensive parameters such as SSA, asymmetry factor and refractive index, the retrieval uncertainties increase rapidly with decreasing AOD: this type of dependence was the motivation behind the Level 2.0 criterion that limits retrievals of these parameters to conditions where AOD(440 nm)>0.4 (Holben et al., 2006). Because of this AOD>0.4 requirement, level 2.0 La Paz data over the whole database were limited to just six retrievals acquired during the 21st to 25th September 2010 period. Thus for this station only, we used Level 1.5 data that fulfilled the Level 2.0 sky conditions - sky errors, solar zenith scattering angle criterion - while constraining the retrievals to AOD values > 0.2. The analyses are only done for the biomass-burning seasons since there are little retrievals during the other seasons. The main statistical parameters of SSA, real and imaginary refractive index and asymmetry factor are listed in Table 4 (for a wavelength at 500 nm from linear interpolation of values at 440 and 670 nm).

[Insert Table 4 here]

From Table 4, SSA is generally lower in the highlands, implying more absorbing particles. The imaginary part of the refractive index exhibits considerably larger values in the

508 highlands (i.e. stronger absorption with imaginary refractive index values that are, except for
509 Cuiba, greater by~ 0.005 than the lowland cases). The real part of the refractive index is
510 approximately the same for the different lowland stations, while the highland station values are
511 significantly higher. Finally, there are differences in the asymmetry factor, mostly in the near
512 infrared region, that are likely related to particle size differences. The changes between the
513 lowland and highland retrieval parameters of Table 4 suggest changes in particle composition
514 (notably the real part of the refractive index).

515 Larger SSA values being associated with the long-range transport of biomass-burning
516 particles is known in the literature (e.g. Colarco et al., 2004). In the case of inter-regional
517 transport between the lowlands and the highlands, the explanation of the differences in particle
518 composition is hypothesized to be the large differences in the availability of water vapor in the
519 atmosphere commented before: hygroscopic particles grow quickly by humidification in the
520 lowlands (see, for e.g. Kotchenruther et al., 1998 and Kreidenweis et al., 2001 for general
521 discussions on humidity induced particle growth of smoke particles). The water vapor condenses
522 on the particles making them larger thereby increasing their scattering efficiency while also
523 decreasing their imaginary refractive index, resulting in making them less absorbing. At higher
524 altitudes, this particle growth effect is less probable due to the less availability of water vapor as
525 well as the fact that the water coatings of particles uplifted from the lowlands may have largely
526 evaporated. In spite of the possible mixture of smoke with local particles, the lower values of the
527 real part of refractive index in the lowlands (~1.47) versus the highlands (~1.53) would support a
528 hypothesis of humidification. It must however be borne in mind that, although humidification of
529 biomass-burning particles affects their properties in general, our retrievals involve column-
530 integrated properties, and we must accordingly be careful to not infer more from those retrievals

than can be justified. Indeed, these limitations indicate that more investigations into smoke dynamics are needed than we carried out in our study. In particular, experimental plans would need to include resources for the measurement of vertical-profiles of aerosol properties such as those performed in the SAFARI-2000 field campaign (Swap et al., 2003), either by airplanes (Hobbs et al., 2003) or lidar measurements (McGill et al., 2003; Veselovskii et al., 2009).

Because SSA is a key aerosol radiative forcing parameter, it is important to study both its spatial and temporal evolution. To that end, Figure 12 shows the mean SSA and AOD means at 500 nm (computed from linear interpolation using 440 and 675 nm values) for the lowland stations and for each biomass-burning season during the 2000-2013 period. The year to year averages of Figure 12a reflect the influence of the day-to-day variations of Figure 2 with, for example, peaks in 2005, 2006, 2007 and 2010 (except that the mean values of Figure 12a seem larger than expected: this is because the inversion processing protocols exclude retrievals for which AOD(440) is less than 0.4).With respect to the SSA, we note significant station-to-station variability in Figure 12b. The SSA analysis reveals curious results: for the large AOD years (2005, 2006, 2007 and 2010) the values of SSA are approximately similar among the stations with an average that is close to 0.90. However, for the years of lower AODs (e.g. 2003, 2004 and 2008), SSA values are lower(0.85 - 0.78)at Cuiaba and Santa Cruz, while at Rio Branco and Ji Parana the values remain around 0.92. During the years of very intense burning activity (2005, 2006, 2007 and 2010) the burned area is very extensive in area: there is accordingly an enormous loading of particles in the atmosphere that arguably produce spatial homogenization of aerosol properties associated with greater regional transport dynamics. For smaller AODs the aerosols are not so regionally homogenous and differences in particle properties can arise between different sites.During low biomass-burning years at the southern Cuiaba and Santa Cruz sites,

554 cerrado and agricultural burning is very likely more dominant. During higher biomass-burning
555 years there would be more long-range transport of higher AOD plumes from the forest burning
556 regions towards the south and west (Freitas et al., 2005). The cerrado vegetation (savannah type)
557 burns with relatively more flaming phase combustion, thereby producing more black carbon.
558 This results in lower SSA than smoke from forest burning regions which have a higher
559 percentage of smoldering phase combustion from woody fuels therefore producing less black
560 carbon(e.g. Ward et al., 1992; Reid et al. 2005a,b).

561 [Insert Figure 12 here]

562 A scatterplot analysis of SSA versus AOD is shown in Figure 13. The large SSA values
563 of approximately 0.90 to 0.95 for very large AOD values are observed again for all the stations.
564 For lower AODs there are, as discussed above, site-dependences with low SSA values in Cuiaba
565 and Santa Cruz and larger values in Ji Parana and Rio Branco. Lower AOD with low SSA is
566 particularly observed in 2008, when an anomaly in the biomass-burning pattern was observed
567 using OMI data (Torres et al., 2010). For that year we note the rather extraordinary AERONET
568 station-to-station SSA differences (which the OMI sensor, with its coarse spatial resolution of 1°
569 x 1°, is largely insensitive to). The fact that the fires were less intense and sparser, and/or that
570 particle-type emission differences occurred between the savannah-like cerrado vegetation and the
571 rainforest, could explain the lack of SSA spatial homogeneity.

572 [Insert Figure 13 here]

573 **3.4. Aerosol transport patterns to the highlands: biomass-burning case study in September-**
574 **October 2010.**

575 Our goal in this section is to illustrate the smoke patterns and transport from the lowlands
576 to the highlands during one carefully analysed biomass-burning season. We particularly

investigated the intense biomass-burning season of September-October 2010 when large AODs (0.5) were registered at La Paz on a few days. Such AODs values are more than three times the average at La Paz. Figure 14 shows the temporal evolution of AOD, α(440-870), r_{eff} and r_{fine} for this case study at the Cuiaba, Ji-Parama, Rio Branco, Santa Cruz and La Paz stations.

[Insert Figure 14 here]

We divided the biomass-burning case study period into five sub-periods. The first subperiod (I) goes from 1 to 18 September and is characterized by strong biomass-burning in the lowlands with AODs of up to 3.2. The Angstrom parameters values of around 1.8 along with $\eta >$ 0.9 indicate a predominance of fine particles. In this period there were no measurements at the La Paz station until 15th September. However, AOD values at La Paz on this day are very low suggesting weak transport of biomass-particles to the Andean Altiplano. The MODIS image for September 17th (Figure 15a) shows the smoke plume had pushed toward the eastern regions (Cuiaba, Ji Parana and Santa Cruz), while the areas close to Rio Branco, the foothills and the highlands, look less turbid.

The second subperiod (II) from 18th to 25th September includes intense biomass-burning events that reach the La Paz region. Smoke plumes can be seen to be bordering the highlands in the MODIS image for 21st September (Figure 15b). In this subperiod, the largest AODs of the entire database at La Paz were registered (up to 0.6), with a mean value of approximately 0.5. An increase in α(440-870) associated with the arrival of fine mode biomass-burning particles is also evident in Figure 14. The values of r_{fine} are relatively small (~0.19 µm), robust and stable (low scatter during this day). After the third day (21st September), the decrease of α(440-870), the increase of r_{eff} and the clear increase of r_{fine} suggest fine mode aerosol aging (maybe

accompanied by the presence of some coarse mode). This could be explained, for example, by the growth effects (such as coagulation) induced by the accumulation of smoke particles over several days (e.g. Reid et al., 2005a,b).

[Insert Figure 14 here]

The study of air-mass transport to the highlands was initially done by computing backward trajectories using HYSPLIT. On 17th September air-masses arriving at 1500 m a.g.l. originated over the Pacific Ocean (the backward-trajectories are provided in the supplement) indicate prevailing westerly winds and explain the movement of the biomass plume towards the East compared to what was observed on previous days. For the intense biomass-burning on 21st September, the backward-trajectories arriving at 750 and 1500 m a.g.l. (graphs in the supplement) encounter the mountains producing an unrealistic calculation since the vertical velocities are essentially zero. The same is observed on 17 September for the 750 m a.g.l. backward-trajectory. To ameliorate this problem, HYSPLIT offers the possibility of coupling backward-trajectory calculations with a Lagrangian dispersion component (Stein et al., 2015). The use of air concentration backward-trajectories allows us to represent the uncertainty in the calculation arising from the model's characterization of the random motions created by atmospheric turbulence. The concentration pattern identifies the potential sources that might have contributed to the particles arriving at the site in question. Figure 16 shows the air concentration of particles at La Paz station for integration periods of 5 days (120 hours). Model initialization heights were 300 and 2000 m a.g.l. (approximately in and above the planetary boundary layer), with a total of 25,000 particles.

[Insert Figure 16 here]

621 Figures 16a and 16b show very similar patterns of the potential sources that could have
622 influenced concentrations at the two representative heights of 300 and 2000 m a.g.l .on 17th
623 September 2010.The largest concentrations are ~ 1E-13 units/m^3 in the area surrounding La Paz.
624 Other potential sources are located in the North and Northeast regions and in the transit area
625 between the highlands and lowlands (foothills that are locally known as 'Las Yungas'). The
626 backward air concentration evaluated every 6 hours (graphs shown in the supplement) reveal that
627 air masses that started in the previous 1-2 days had their origin in the region close to La Paz
628 while those further from the North and the Pacific Ocean are from the last 4-5 days. Such
629 complex patterns of air concentration are associated with the westerly winds from the Pacific at
630 high altitudes (> 1500 m a.g.l.) and slow winds at low altitudes (< 750 m a.g.l.).

631 Figures16cand 16d also show similar patterns for the two levels on 21th September 2010,
632 with almost no particles transported from the west region while the largest potential sources are
633 in the Amazonian lowlands to the east. Long-range transport is observed from the eastern regions
634 of Bolivia and its border with Brazil, and even, for the 300 m a.g.l. level, from more distant areas
635 in Brazil, northern Paraguay and Argentina. The backward air concentration evaluations for
636 every 6 hours (graphs shown in the supplement) reveal that the areas with lower concentrations
637 correspond approximately to the previous 3-5 days while larger concentration areas correspond
638 to the previous 1-3 days.

639 Figure 17 shows CALIPSO lidar attenuated backscatter at 532 nm and vertical feature
640 mask for 20th September 2010 when the instrument passed over South America close to the study
641 region. The plot also shows the mean height above sea level. For the study region we observe
642 intense attenuated backscatter that is classified by the feature mask algorithm (Omar et al., 2009)
643 as tropospheric aerosol. According to our analyses of Figure 15 and 16 such aerosol particles

correspond to smoke particles. The attenuated backscatter values are close to that found in the literature for smoke particles in Amazonia (e.g. Baars et al., 2012). It is clearly seen that the mountains act as a natural barrier, with aerosol accumulating in the lowlands along the southern and northern sides of the Andes Mountains. It is also observed that smoke plumes can reach the high mountains, but with considerably lower amounts than in the lowlands. In fact, some of these plumes have AOD values close to the detection limit of CALIPSO. All these findings agree with our general analyses of smoke particles transported to Andean high mountains. Unfortunately, CALIPSO did not cross over La Paz during the days of interest to this study and no direct comparison with this station could be done.

[Insert Figure 17 here]

The third subperiod (III) from 26th to 29th September is also characterized by air-masses with origins in the Pacific Ocean (backward-trajectories not shown). Very low AODs were registered again in Rio Branco and La Paz (the western locations) and the MODIS image (Figure 15c) shows that the smoke particles have apparently moved toward the east relative to the MODIS image of Figure 15b. These findings again support the notion that strong westerly winds cleaned the atmosphere. Large highland variability in $\alpha(440\text{-}870)$, r_{eff} and r_{fine}, associated with large uncertainties for low aerosol loads, is observed again. The presence of coarse mode particles at the highland station is again inferred from smaller values of $\alpha(440\text{-}870)$ and larger values of r_{eff}. The situation is however different to the East as indicated by the large AODs in Cuiaba.

The fourth subperiod (IV) extends from 30th September to 3rd October and is characterized by a change of the air-mass origin towards the northeast in the vicinity of Peru. For

this case backward-trajectories (graphs included in the supplement) are not adversely affected by the high mountains as they were for the other dates. During this period the most relevant factor is the significant amount of cloud cover (as observed in the MODIS image of Figure 15d) both in the Pacific and in the Amazonia basin.

The last subperiods (V & VI) of Figure 14 extends from 3rd to 31st October and was generally characterized by the two different air-mass patterns identified above. In this subperiod we note the considerably lower aerosol load at all the stations compared to the values registered in September. In general the atmosphere was clean during this subperiod as illustrated by the MODIS image on the 5th of October (Figure 15e). For this day, air-masses encountered the mountains and the backward dispersion air concentrations were again employed (see graphs in the supplement), with patterns similar to these of Figures 16a and 16b and particles originating from the northwest and southwest highlands and the Pacific Ocean. Therefore, no transport of biomass-burning to La Paz was expected on October 5th, which is consistent with the weak AODs of Figure 14 and the MODIS image (Figure 15e). On the other hand, between 10th and 15th October were registered sparse lowland biomass-burning events with some AODs above 0.4, high values of α(440-870) (close to 1.8) and stable values of r_{eff} and r_{fine} of 0.22 and 0.19 µm. The MODIS Aqua image for October 13th (Figure 15f) supports the characterization of "sparse" and shows more intense and homogeneous biomass-burning plumes to the east of La Paz. Air concentration backward-trajectory analyses were again required: the long-range transport from the lowlands in the Amazon is similar to that observed for the intense smoke events of the 20th September at La Paz (see graphs in the supplement). In this case, however, no important AOD enhancement was registered at the La Paz station. The main reason for this is

likely the sparse (and probably low intensity) nature of fires in the lowlands during the 10th-15th October period.

An analysis of wind regimes over La Paz for the August-October 2010 period reveals that, at the 750 and 1500 m a.g.l. levels, 16-22% of the cases were associated with westerly winds, while the rest (percentages around 80 %) were associated with easterly winds originated in the lowlands at the Amazonia. Although the analyses were for the particular biomass-burning season of 2010, the results may be representative of the general patterns that favour/suppress the transport of smoke particles in the tropical Andean region. More in depth studies would require the use of very high temporal-resolution meteorological data, and a large dataset of meteorological variable measurements for a more comprehensive evaluation of these patterns. Profile analyses using active remote sensing measurements are also required (e.g. multiwavelength lidar) to better understand the vertical profile of the transported smoke particles.

4.- Conclusions

We carried out an analysis of columnar aerosol properties in the South American tropical region within 10-20° South and 50-70° West. The area includes the Amazon (lowlands), the high mountain regions (highlands) and the transition between the two (foothills). Precipitation in the region occurs mainly in the December-March period while the June-October period is very dry. The most important geo-atmospheric factor is the strong altitude gradient between the lowlands and the highlands, which implies change in vegetation and in water vapor concentration. The contrast of aerosol properties between the lowlands and highlands is studied using the 2000-2014

AERONET measurements across the lowland stations of Rio Branco, Ji Parana, Cuiaba (stations in Brazil) and Santa Cruz (Bolivia) and the highlands station of La Paz (Bolivia).

For the lowlands, an enhanced annual cycle in aerosol optical depth (AODs) and Angstrom parameter (α(440-870)) was observed during the biomass-burning season (August-October) across all the stations. Year to year variability, with maximum AODs in 2005, 2006, 2007 and 2010 was observed and directly linked to biomass burning activity. Using TRMM satellite data, precipitation links were studied within the context of precipitation anomalies defined as the difference between annual and climatological values for the wet (November-March) dry (April-July) and biomass-burning (August-October) seasons. Positive anomalies during the wet season influence the amount of vegetation available to be burned, while negative anomalies in the dry period favours fire activity. This hypothesis was found for the intense biomass-burning seasons in 2005, 2006, 2007 and 2010, while the opposite happens in 2009 with lower fire activity. After 2010, however, we did not observe such links with precipitation. Other factors, such as the influence of government policies on burning practices could have had an impact on our proposed relationship between rainfall anomaly and AOD and thus future investigations are needed.

The analyses during the biomass-burning season in the lowlands showed, as expected, a large predominance of fine mode particles. We also demonstrated an increase, predominantly in the fine mode, of particle radius, as AOD increases. This demonstration was achieved because we used the much more numerous retrievals of particle radius from spectral AOD measurements in spite of the larger uncertainties compared to AERONET standard retrievals. Such a finding is likely associated with the accumulation of particles. The study of the single scattering albedo (SSA) also revealed interesting findings: for the years of intense biomass-burning activity, values

of SSA (~ 0.93) are homogeneous with very similar values among all the stations. However, for the years with less intense activity, such as 2008, intra-lowland differences arise with the SSA being larger (~0.95) at the northern stations of Rio Branco and Ji Parana and lower at the southern stations of Cuiaba and Santa Cruz (SSA values with mean of ~ 0.85 and minimum values even below 0.75). In the northern locations, the biomass burning of the rainforest predominates while in the other locations cerrado and agricultural burning is more dominant. The type of vegetation/rainforest burned could explain some of the differences observed in SSA. More investigation is needed to confirm or reject this hypothesis.

The La Paz highlands data also showed an annual AOD cycle with maximums during the biomass-burning season. These maximum values, ranging up to 0.5, are high for this region where the mean AOD is approximately 0.12. Ongoing studies with in-situ instrumentation are revealing the presence of anthropogenic particles during the whole year, and the only sources in the Bolvian Altiplano of such particles are the local industry and road traffic in the La Paz region. Also, the natural sources of highland aerosols are associated with dust from the Altiplano, which is present during the whole year. Therefore, the seasonal enhancement of AOD is associated with the transport of lowland smoke. However, it was found that this transport is sporadic in nature. Highland particle radii showed important differences compared to lowland values: For the effective radius (r_{eff}), which is sensitive to fine and coarse particles, systematically larger La Paz values were likely influenced by the continuous presence of dust particles from the Altiplano. The lowland station of Santa Cruz has shown the presence of coarse particles which we suggested was associated with wind-driven river bed erosion. Systematically larger values of fine mode radius (r_{fine}) were observed at La Paz over the whole year. Because changes in r_{fine} are attributable to changes in the fine mode, these differences were thought to be

due to fine mode particle aging, a mechanism that is probably favoured by the high mountain wind regimes. Transport of smoke particles to the highlands was associated with larger highland values of particle size (both r_{fine} and r_{eff} were larger) whose growth was attributed to particle aging.

The transported smoke particles to the highlands had lower values of SSA: large relative (and specific) humidity in the lowlands favours particle growth by hygroscopicity with an attendant decrease in optical absorption. In the highlands, however, relative (and specific) humidity is quite low and it is likely that water, previously absorbed by the particles, evaporates. The SSA retrieval numbers are, however, relatively small and it has not been possible to verify this hypothesis. Comprehensive field campaigns will be needed to further identify the impact of transported biomass-burning particles, preferably including simultaneous lowland and highland measurements. These kinds of investigations are desired as future activities of the Global Atmospheric Watch activities focussed on the station at Mount Chacaltaya(5240 m a.s.l.) in Bolivia.

The analyses of the air-masses reaching the station of La Paz were carried out using the HYSPLIT model. It has been found that the computed flow of backward-trajectories frequently encounters mountains, thus introducing large uncertainties in the backward-trajectory computations. Indeed, the HYSPLIT air concentration backward-dispersion has been used to identify the potential sources that might have contributed to the particles arriving at the site in question. The analyses of air concentration backward-dispersion have revealed that easterly winds predominate allow the transport of biomass-burning particles from the Amazonian lowlands, including regions of eastern Brazil, northern Paraguay and northern Argentina to the highlands. On the other hand, westerly winds help to clean the atmosphere. HYSPLIT allow

being coupled with mesoscale models such as the Weather and Research Forecast (WRF) model, and that will allow the identification of detailed transport of pollutants through the mountains. Such advances are necessary for better understanding the vulnerability of the Andean high mountain regions to climate change. These climate-driven studies must be combined with others in glaciology to study water resources, water quality and water use efficiency, and will support environmental and economic development of the nations of the Andean regions.

Acknowledgments

This work was supported by the Marie Skłodowska-Curie Individual Fellowships (IF) ACE_GFAT (grant agreement No 659398), by the Postdoctoral Program of the University of Granada,by the NASA Atmospheric Composition Program and by the NASA Aerosols, Clouds, Ecosystems mission. The authors thankfully acknowledge the AERONET team for maintaining the stations used in this work and to the NOAA Air Research Laboratory for providing the HYSPLIT model.

References

Alados-Arboledas, L., Müller, D., Guerrero-Rascado, J.L., Navas-Guzmán, F., Pérez-Ramírez, D., Olmo, F.J. (2011) Optical and microphysical properties of fresh biomass burning aerosol retrieved by Raman lidar, and star-and sun-photometry. Geophysical Research Letters 38.

Alastuey, A. (2017) Measurements of PM10 and PM2.5 at the Bolivian Andean Altiplano and in La Paz region. Personal Communication, Chacaltaya GAW station Scientific Steering Committee, 7 June 2017, La Paz, Bolivia.

Andreae, M.O., Merlet, P. (2001) Emission of trace gases and aerosols from biomass burning. Global Biogeochemical Cycles 15, 955-966.

807 Baars, H., Ansmann, A., Althausen, D., Engelmann, R., Heese, B., Müller, D., Artaxo, P.,
808 Paixao, M., Pauliquevis, T., Souza, R. (2012) Aerosol profiling with lidar in the Amazon
809 Basin during the wet and dry season. Journal of Geophysical Research: Atmospheres 117,
810 n/a-n/a.
811
812 Bonasoni, P., Laj, P., Marinoni, A., Sprenger, M., Angelini, F., Arduini, J., Bonafè, U.,
813 Calzolari, F., Colombo, T., Decesari, S., Di Biagio, C., di Sarra, A.G., Evangelisti, F., Duchi, R.,
814 Facchini, M.C., Fuzzi, S., Gobbi, G.P., Maione, M., Panday, A., Roccato, F., Sellegri, K., Venzac,
815 H., Verza, G.P., Villani, P., Vuillermoz, E., Cristofanelli, P. (2010) Atmospheric Brown Clouds
816 in the Himalayas: first two years of continuous observations at the Nepal Climate
817 Observatory-Pyramid (5079 m). Atmospheric Chemistry and Physics 10, 7515-7531.
818
819 Bond, T.C., Doherty, S.J., Fahey, D.W., Forster, P.M., Berntsen, T., DeAngelo, B.J.,
820 Flanner, M.G., Ghan, S., Kärcher, B., Koch, D., Kinne, S., Kondo, Y., Quinn, P.K., Sarofim, M.C.,
821 Schultz, M.G., Schulz, M., Venkataraman, C., Zhang, H., Zhang, S., Bellouin, N., Guttikunda,
822 S.K., Hopke, P.K., Jacobson, M.Z., Kaiser, J.W., Klimont, Z., Lohmann, U., Schwarz, J.P.,
823 Shindell, D., Storelvmo, T., Warren, S.G., Zender, C.S. (2013) Bounding the role of black
824 carbon in the climate system: A scientific assessment. Journal of Geophysical Research:
825 Atmospheres 118, 5380-5552.
826
827 Boucher, E.H., and Stein, A.F. (2016). Large salt dust storms follow a 30-year rainfall
828 cycle in the Mar Chiquita Lake (Córdoba, Argentina). PLos ONE, 11(6): e0156672, doi:10.1371-
829 journal.pone.0156672.

830 Bourgeois, Q., Ekman, A.M.L., Krejci, R. (2015) Aerosol transport over the Andes
831 from the Amazon Basin to the remote Pacific Ocean: A multiyear CALIOP assessment.
832 Journal of Geophysical Research: Atmospheres 120, 8411-8425.
833
834 Bowman, D.M.J.S., Balch, J.K., Artaxo, P., Bond, W.J., Carlson, J.M., Cochrane, M.A.,
835 D'Antonio, C.M., DeFries, R.S., Doyle, J.C., Harrison, S.P., Johnston, F.H., Keeley, J.E.,
836 Krawchuk, M.A., Kull, A.C., Marston, J.B., Moritz, M.A., Prentice, I.C., Roos, C.I., Scott, A.C.,
837 Swetnam, T.W., van der Werf, G.R., Pyne, S.J. (2009) Fire in the Earth System. Science 324,
838 481-484.
839
840 Bowman, D.M.J.S., Johnston, F.H. (2005) Wildfire smoke, fire management, and
841 human health. EcoHealth 2, 76-80.
842
843 Colarco, P.R., Toon, O.B., Holben, B.N. (2003) Saharan dust transport to the
844 Caribbean during PRIDE: 1. Influence of dust sources and removal mechanisms on the
845 timing and magnitude of downwind aerosol optical depth events from simulations of in situ
846 and remote sensing observations. Journal of Geophysical Research 108, 8589.
847
848 Colarco, P.R., Schoeberl, M.R., Doddridge, B.G., Marufu, L.T., Torres, O., Welton, E.J.
849 (2004) Transport of smoke from Canadian forest fires to the surface near Washington, D.C.:
850 Injection height, entrainment, and optical properties. Journal of Geophysical Research 109.

Crusius, J., Schroth, A.W., Gassó, S., Moy, C.M., Levy, R.C., and Gatica, M. (2011) Glacial flourduststorms in theGulf of Alaska: Hydrologic and meteorologicalcontrols and theirimportance as a source of bioavailableiron. GeophysicalResearchLetters, 38, L06602

Dubovik, O., King, M.D. (2000) A flexible inversion algorithm for retrieval of aerosol optical properties from Sun and sky radiance measurements. Journal of Geophysical Research 105, 20673-20696.

Dubovik, O., Holben, B., Eck, T.F., Smirnov, A., Kaufman, Y.J., King, M.D., Tanre, D., Slutsker, I. (2002) Variability of absorption and optical properties of key aerosol types observed in worldwide locations Journal of the Atmospheric Sciences 59, 590-608.

Dubovik, O., Sinyuk, A., Lapyonok, T., Holben, B.N., Mishchenko, M., Yang, P., Eck, T.F., Volten, H., Muñoz, O., Veihelmann, B., van der Zande, W.J., Leon, J.-F., Sorokin, M., Slutsker, I. (2006) Application of spheroid models to account for aerosol particle nonsphericity in remote sensing of desert dust. Journal of Geophysical Research 111, D11208.

Dumka, U.C., Moorthy, K.K., Satheesh, S.K., Sagar, R., Pant, P. (2008) Short-Period Modulations in Aerosol Optical Depths over the Central Himalayas: Role of Mesoscale Processes. Journal of Applied Meteorology and Climatology 47, 1467-1475.

Eck, T.F., Holben, B.N., Reid, J.S., Dubovik, O., Smirnov, A., O'Neill, N.T., Slutsker, I., Kinne, S. (1999) Wavelength dependence of the optical depth of biomass burning, urban, and desert dust aerosols. Journal of Geophysical Research 104, 31333-31349.

Eck, T.F., Holben, B.N., Ward, D.E., Mukelabai, M.M., Dubovik, O., Smirnov, A., Schafer, J.S., Hsu, N.C., Piketh, S.J., Queface, A., Le Roux, J., Swap, R.J., Slutsker, I. (2003) Variability of biomass burning aerosol optical characteristics in southern Africa during the SAFARI 2000 dry season campaign and a comparison of single scattering albedo estimates from radiometric measurements. Journal of Geophysical Research 108.

Eck, T.F., Holben, B.N., Reid, J.S., Sinyuk, A., Hyer, E.J., O'Neill, N.T., Shaw, G.E., Vande Castle, J.R., Chapin, F.S., Dubovik, O., Smirnov, A., Vermote, E., Schafer, J.S., Giles, D., Slutsker, I., Sorokine, M., Newcomb, W.W. (2009) Optical properties of boreal region biomass burning aerosols in central Alaska and seasonal variation of aerosol optical depth at an Arctic coastal site. Journal of Geophysical Research 114.

Eck, T.F., Holben, B.N., Sinyuk, A., Pinker, R.T., Goloub, P., Chen, H., Chatenet, B., Li, Z., Singh, R.P., Tripathi, S.N., Reid, J.S., Giles, D.M., Dubovik, O., O'Neill, N.T., Smirnov, A., Wang, P., Xia, X. (2010) Climatological aspects of the optical properties of fine/coarse mode aerosol mixtures. Journal of Geophysical Research 115, D19205.

Eck, T.F., Holben, B.N., Reid, J.S., Mukelabai, M.M., Piketh, S.J., Torres, O., Jethva, H.T., Hyer, E.J., Ward, D.E., Dubovik, O., Sinyuk, A., Schafer, J.S., Giles, D.M., Sorokin, M., Smirnov, A., Slutsker, I. (2013) A seasonal trend of single scattering albedo in southern African

biomass-burning particles: Implications for satellite products and estimates of emissions for the world's largest biomass-burning source. Journal of Geophysical Research: Atmospheres 118, 6414-6432.

Eck, T., Holben, B., Giles, D., Smirnov, A., Slutsker, I., Sinyuk, A., Schafer, J., Sorokin, M., Reid, J., Sayer, A., Hsu, C., Levy, R., Lyapustin, A., Wang, Y., Rahman, M.A., Liew, S.-C., Salinas Cortijo, S.V., Li, T., Kalbermatter, D., Keong, K.L., Elifant, M., Aditya, F., Mohamad, M., Chong, T.K., San, L.H., Choon, Y.E., Deranadyan, G., Kusumanigtyas, S., Mahmud, M. (2016) Remote sensing measurements of biomass burning aerosol optical properties during the 2015 Indonesian burning season from AERONET and MODIS satellite data. In "Remote Sensing of Clouds and Aerosols: Techniques and Applications", European Geosciences Union General Assembly 2016, Vienna, Austria 17-22 April 2016. online available in http://meetingorganizer.copernicus.org/EGU2016/EGU2016-2391-3.pdf.

Freitas, S.R., Longo, K., Silva Dias, M.A.F., Silva Dias, P.L., Chatfield, R., Prins, E., Artaxo, P., Grell, G.A., Recuero, F.S. (2005) Monitoring the transport of biomass burning emissions in South America. Environmental Fluid Mechanics 5, 135-167.

Gaiero, D.M., Simonella, L., Gassó, S., Gili, S., Stein, A.F., Sosa, P., Becchio, R., Arce, J., and Marelli, H. (2013). Ground/satellite observations and atmospheric modeling of dust storms originating in the high Puna-Altiplano deserts (South America): Implications for the interpretation of paleo-climate archives. Journal of Geophysical Research: Atmospheres, 118, 3817-3831.

Gautam, R., Hsu, N.C., Tsay, S.C., Lau, K.M., Holben, B., Bell, S., Smirnov, A., Li, C., Hansell, R., Ji, Q., Payra, S., Aryal, D., Kayastha, R., Kim, K.M. (2011) Accumulation of aerosols over the Indo-Gangetic plains and southern slopes of the Himalayas: distribution, properties and radiative effects during the 2009 pre-monsoon season. Atmospheric Chemistry and Physics 11, 12841-12863.

Guirado, C., Cuevas, E., Cachorro, V.E., Toledano, C., Alonso-Pérez, S., Bustos, J.J., Basart, S., Romero, P.M., Camino, C., Mimouni, M., Zeudmi, L., Goloub, P., Baldasano, J.M., de Frutos, A.M. (2014) Aerosol characterization at the Saharan AERONET site Tamanrasset. Atmospheric Chemistry and Physics 14, 11753-11773.

Hobbs, P.V., Sinha, P., Yokelson, R.J., Christian, T.J., Blake, D.R., Gao, S., Kirchstetter, T.W., Novakov, T., Pilewskie, P. (2003) Evolution of gases and particles from a savanna fire in South Africa. Journal of Geophysical Research 108, 8485.

Holben, B.N., Eck, T.F., Slutsker, I., Tanre, D., Buis, J.P., Setzer, A., Vermote, E., Reagan, J.A., Kaufman, Y.J., Nakajima, T., Lavenu, F., Jankowiak, I., Smirnov, A. (1998) AERONET- A federated instrument network and data archive for aerosol characterization. Remote Sensing of Environment 66, 1-16.

940 Holben, B.N., Eck, T.F., Slutsker, I., Smirnov, A., Sinyuk, A., Schafer, J., Giles, D.,
941 Dubovik, O. (2006) Aeronet's Version 2.0 quality assurance criteria. Proceedings of SPIE
942 6408, 64080Q.
943
944 Jacobson, M.Z. (2014) Effects of biomass burning on climate, accounting for heat and
945 moisture fluxes, black and brown carbon, and cloud absorption effects. Journal of
946 Geophysical Research: Atmospheres 119, 8980-9002.
947
948 Kim, D., Chin, M., Yu, H., Eck, T.F., Sinyuk, A., Smirnov, A., Holben, B.N. (2011) Dust
949 optical properties over North Africa and Arabian Peninsula derived from the AERONET
950 dataset. Atmospheric Chemistry and Physics 11, 10733-10741.
951
952 Koren, I., Remer, L.A., Longo, K.M. (2007) Reversal of trend of biomass burning in
953 the Amazon. Geophysical Research Letters 34, L20404.
954
955 Koren, I., Martins, J.V., Remer, L.A., Afargan, H. (2008) Smoke invigoration versus
956 inhibition of clouds over the Amazon. Science 321, 946-949.
957
958 Koren, I., Remer, L.A., Longo, K., Brown, F., Lindsey, R. (2009) Reply to comment by
959 W. Schroeder et al. on "Reversal of trend of biomass burning in the Amazon". Geophysical
960 Research Letters 36, L03807.
961
962 Kotchenruther, R.A., Hobbs, P.V. (1998) Humidification factors of aerosols from
963 biomass burning in Brazil. Journal of Geophysical Research 103, 32081-32089.
964
965 Kreidenweis, S.M., Remer, L.A., Bruintjes, R., Dubovik, O. (2001) Smoke aerosol from
966 biomass burning in Mexico: Hygroscopic smoke optical model. Journal of Geophysical
967 Research 106, 4831-4844.
968
969 Latrubesse, E.M., Stevaux, J.C., Cremon, E.H., May, J.-H., Tatumi, S.H., Hurtado, M.A.,
970 Bezada, M., Argollo, J.B. (2012). Late Quaternary megafans, fans and fluvio-aeolian interactions
971 in the Bolivian Chaco, Tropical South America. Paleogeography, Paleoclimatology,
972 Palaeoecology, 356-357, 75-88.

973 Longo, K.M., Freitas, S.R., Andreae, M.O., Setzer, A., Prins, E., Artaxo, P. (2010) The
974 Coupled Aerosol and Tracer Transport model to the Brazilian developments on the
975 Regional Atmospheric Modeling System (CATT-BRAMS) – Part 2: Model sensitivity to the
976 biomass burning inventories. Atmospheric Chemistry and Physics 10, 5785-5795.
977
978 Lüthi, Z.L., Škerlak, B., Kim, S.W., Lauer, A., Mues, A., Rupakheti, M., Kang, S. (2015)
979 Atmospheric brown clouds reach the Tibetan Plateau by crossing the Himalayas.
980 Atmospheric Chemistry and Physics 15, 6007-6021.
981
982 Maione, M., Giostra, U., Arduini, J., Furlani, F., Bonasoni, P., Cristofanelli, P., Laj, P.,
983 Vuillermoz, E. (2011) Three-year observations of halocarbons at the Nepal Climate

Observatory at Pyramid (NCO-P, 5079 m a.s.l.) on the Himalayan range. Atmospheric Chemistry and Physics 11, 3431-3441.

Marcq, S., Laj, P., Roger, J.C., Villani, P., Sellegri, K., Bonasoni, P., Marinoni, A., Cristofanelli, P., Verza, G.P., Bergin, M. (2010) Aerosol optical properties and radiative forcing in the high Himalaya based on measurements at the Nepal Climate Observatory-Pyramid site (5079 m a.s.l.). Atmospheric Chemistry and Physics 10, 5859-5872.

Matichuk, R.I., Colarco, P.R., Smith, J.A., Toon, O.B. (2008) Modeling the transport and optical properties of smoke plumes from South American biomass burning. Journal of Geophysical Research 113.

McGill, M.J., Hlavka, D.L., Hart, W.D., Welton, E.J., Campbell, J.R. (2003) Airborne lidar measurements of aerosol optical properties during SAFARI-2000. Journal of Geophysical Research 108, 8493.

Mishra, A.K., Lehahn, Y., Rudich, Y., Koren, I. (2015) Co-variability of smoke and fire in the Amazon basin. Atmospheric Environment 109, 97-104

Morton, D.C., Defries, R.S., Randerson, J.T., Giglio, L., Schroeder, W., Van Der Werf, G.R. (2008) Agricultural intensification increases deforestation fire activity in Amazonia. Global Change Biology 14, 2262-2275.

Nogues-Paegle, J., Mo, K. (1997) Alternating wet and dry conditions over South America during summer. Monthly Weather Review 125.

Noh, Y.M., Müller, D., Shin, D.H., Lee, H., Jung, J.S., Lee, K.H., Cribb, M., Li, Z., Kim, Y.J. (2009) Optical and microphysical properties of severe haze and smoke aerosol measured by integrated remote sensing techniques in Gwangju, Korea. Atmospheric Environment 43, 879-888.

Omar, A. H., Winker, D. M., Kittaka, C., Vaughan, M. A., Liu, Z., Hu, Y., and Hostetler, C. A.. (2009) The CALIPSO automated aerosol classification and lidar ratio selectionalgorithm, Journal of Atmospheric and OceanicTechniques, 26, 1994–2014, 2009.

O'Neill, N.T., Dubovik, O., Eck, T.F. (2001a) Applied Optics. Modified Ångstrom exponent for the characterization of submicrometer aerosols 40, 2368-2375.

O'Neill, N.T., Eck, T.F., Holben, B.N., Smirnov, A., Dubovik, O., Royer, A. (2001b) Bimodal size distribution influences on the variation of Angstrom derivatives in spectral optical depth space. Journal of Geophysical Research 106.

O'Neill, N.T., Eck, T.F., Smirnov, A., Holben, B.N., Thulasiraman, S. (2003) Spectral discrimination of coarse and fine mode optical depth. Journal of Geophysical Research 108.

O'Neill, N.T., Thulasiraman, S., Eck, T.F., Reid, J.S. (2005) Robust optical features of fine mode size distributions: Application to the Québec smoke event of 2002. Journal of Geophysical Research 110, D011207.

O' Neill, N.T., Thulasiraman, S., Eck, T.F., Reid, J.S. (2008a) Correction to "Robust optical features of fine mode size distributions: Application to the Québec smoke event of 2002". Journal of Geophysical Research 113, D24203.

O'Neill, N.T., Pancrati, O., Baibakov, K., Eloranta, E., Batchelor, R.L., Freemantle, J., McArthur, L.J.B., Strong, K., Lindenmaier, R. (2008b) Occurrence of weak, sub-micron, tropospheric aerosol events at high Arctic latitudes. Geophysical Research Letters 35.

Pérez-Ramírez, D., Aceituno, J., Ruiz, B., Olmo, F., Alados-Arboledas, L. (2008) Development and calibration of a star photometer to measure the aerosol optical depth: Smoke observations at a high mountain site. Atmospheric Environment 42, 2733-2738.

Pérez-Ramírez, D., Lyamani, H., Olmo, F.J., Whiteman, D.N., Alados-Arboledas, L. (2012) Columnar aerosol properties from sun-and-star photometry: statistical comparisons and day-to-night dynamic. Atmospheric Chemistry and Physics, 12, 9719-9738.

Pérez-Ramírez, D., Veselovskii, I., Whiteman, D.N., Suvorina, A., Korenskiy, M., Kolgotin, A., Holben, B., Dubovik, O., Siniuk, A., Alados-Arboledas, L. (2015) High temporal resolution estimates of columnar aerosol microphysical parameters from spectrum of aerosol optical depth by linear estimation: application to long-term AERONET and star-photometry measurements. Atmospheric Measurement Techniques 8, 3117-3133.

Queface, A.J., Piketh, S.J., Eck, T.F., Tsay, S.-C., Mavume, A.F. (2011) Climatology of aerosol optical properties in Southern Africa. Atmospheric Environment 45, 2910-2921.

Reid, J.S., Hobbs, P.V., Ferek, R.J., Blake, D.R., Martins, J.V., Dunlap, M.R., Liousse, C. (1998) Physical, chemical, and optical properties of regional hazes dominated by smoke in Brazil. Journal of Geophysical Research 103.

Reid, J.S., Eck, T.F., Christopher, S.A., Hobbs, P.V., Holben, B.N. (1999) Use of the Angstrom exponent to estimate the variability of optical and physical properties of aging smoke particles in Brazil. Journal of Geophysical Research 104.

Reid, J.S., Eck, T.F., Christopher, S.A., Koppmann, R., Dubovik, O., Eleuterio, D.P., Holben, B.N., Reid, E.A., Zhang, J. (2005a) A review of biomass burning emissions part III: intensive optical properties of biomass burning particles. Atmospheric Chemistry and Physics 5, 827-849.

Reid, J.S., Koppmann, R., Eck, T.F., Eleuterio, D.P. (2005b) A review of biomass burning emissions part II: intensive physical properties of biomass burning particles. Atmospheric Chemistry and Physics 5, 799-825.

Remy, S., Kaiser, J.W. (2014) Daily global fire radiative power fields estimation from one or two MODIS instruments. Atmospheric Chemistry and Physics 14, 13377-13390.

Sayer, A.M., Hsu, N.C., Eck, T.F., Smirnov, A., Holben, B.N. (2014) AERONET-based models of smoke-dominated aerosol near source regions and transported over oceans, and implications for satellite retrievals of aerosol optical depth. Atmospheric Chemistry and Physics 14, 11493-11523.

Schafer, J.S., Eck, T.F., Holben, B.N., Artaxo, P., Duarte, A.F. (2008) Characterization of the optical properties of atmospheric aerosols in Amazônia from long-term AERONET monitoring (1993–1995 and 1999–2006). Journal of Geophysical Research 113.

Schwikowski, M., Brütsch, S., Gäggeler, H.W., Schotterer, U. (1999) A high-resolution air chemistry record from an Alpine ice core: Fiescherhorn glacier, Swiss Alps. Journal of Geophysical Research: Atmospheres 104, 13709-13719.

Smirnov, A., Holben, B.N., Eck, T.F., Dubovik, O., Slutsker, I. (2000) Cloud-screening and quality control algorithms for the AERONET database. Remote Sensing of Environment 73, 337-349.

Sinyuk, A., Holben, B.N., Smirnov, A., Eck, T.F., Slutsker, I., Schafer, J.S., Giles, D.M., Sorokin, M. (2012) Assessment of error in aerosol optical depth measured by AERONET due to aerosol forward scattering. Geophysical Research Letters 39, L23806.

Stein, A.F., Draxler, R.R., Rolph, G.D., Stunder, B.J.B., Cohen, M.D., Ngan, F. (2015) NOAA's HYSPLIT Atmospheric Transport and Dispersion Modeling System. Bulletin of the American Meteorological Society 96, 2059-2077.

Swap, R.J., Annegarn, H.J., Suttles, J.T., King, M.D., Platnick, S., Privette, J.L., Scholes, R.J. (2003) Africa burning: A thematic analysis of the Southern African Regional Science Initiative (SAFARI 2000). Journal of Geophysical Research: Atmospheres 108, n/a-n/a.

Torres, O., Chen, Z., Jethva, H., Ahn, C., Freitas, S.R., Barthia, P.K. (2010) OMI and MODIS observations of the anomalous 2008-2009 Southern Hemisphere biomass burning seasons. Atmospheric Chemistry and Physics 10, 3505-3513.

Uhl, C., Kauffman, J.B., Cummings, D.L. (1998) Fire in Venezuelan Amazon 2: Environmental conditions necessary for forest fires in the evergreen rainforest of Venezuela. Oikos 53, 176-184.

Ulke, A.G., Longo, K.M., Freitas, S.R., (2011) Biomass burning in south America: transport patterns and impacts., in: Matovic, D. (Ed.), Biomass - Detection, Production and ussage.

Uriarte, M., Yackulic, C.B., Cooper, T., Flynn, D., Cortes, M., Crk, T., Cullman, G., McGinty, M., Sircely, J. (2009) Expansion of sugarcane production in São Paulo, Brazil: Implications for fire occurrence and respiratory health. Agriculture, Ecosystems & Environment 132, 48-56.

van der Werf, G.R., Randerson, J.T., Giglio, L., Collatz, G.J., Mu, M., Kasibhatla, P.S., Morton, D.C., DeFries, R.S., Jin, Y., van Leeuwen, T.T. (2010) Global fire emissions and the contribution of deforestation, savanna, forest, agricultural, and peat fires (1997–2009). Atmospheric Chemistry and Physics 10, 11707-11735.

Van Marle, M.J.E., Field, R., van der Werf, G.R., Estrada de Wagt, I.A., Houghton, R.A., Rizzo, L.V., Artaxo, P., and Tsigaridis, K. (2016) Fire and deforestation dynamics in Amazonia (1973-2014). Global Biogeochemical Cycles, 31, doi:10.1002/2016GB005445.

Vedal, S., Dutton, S.J. (2006) Wildfire air pollution and daily mortality in a large urban area. Environ Res 102, 29-35.

Veselovskii, I., Dubovik, O., Kolgotin, A., Korenskiy, M., Whiteman, D.N., Allakhverdiev, K., Huseyinoglu, F. (2012) Linear estimation of particle bulk parameters from multi-wavelength lidar measurements. Atmospheric Measurement Techniques 5, 1135-1145.

Veselovskii, I., Whiteman, D.N., Korenskiy, M., Kolgotin, A., Dubovik, O., Perez-Ramirez, D., Suvorina, A. (2013) Retrieval of spatio-temporal distributions of particle parameters from multiwavelength lidar measurements using the linear estimation technique and comparison with AERONET. Atmospheric Measurement Techniques 6, 2671-2682.

Veselovskii, I., Whiteman, D.N., Korenskiy, M., Suvorina, A., Kolgotin, A., Lyapustin, A., Wang, Y., Chin, M., Bian, H., Kucsera, T.L., Pérez-Ramírez, D., Holben, B. (2015) Characterization of forest fire smoke event near Washington, DC in summer 2013 with multi-wavelength lidar. Atmospheric Chemistry and Physics 15, 1647-1660.

Vuille, M. (1999) Atmospheric circulation over the Bolivian Altiplano during dry and wet periods and extreme phases of the southern oscillation. International Journal of Climatology, 19, 1579-1600.

Ward, D.E., Susott, R.A., Kauffman, J.B., Babbitt, R.E., Cummings, D.L., Dias, B., Holben, B.N., Kaufman, Y.J., Rasmussen, R.A., and Setzer, W. (1992) Smoke and fire characteristics for cerrado and deforestation burns in Brazil: BASE-B Experiment. Journal of Geophysical Research, 97, 14601-14619.

1162 Wonsick, M.M., Pinker, R.T., Ma, Y. (2014) Investigation of the "elevated heat pump"
1163 hypothesis of the Asian monsoon using satellite observations. Atmospheric Chemistry and
1164 Physics 14, 8749-8761.
1165

1166 Xu, Y., Ramanathan, V., Washington, W.M. (2016) Observed high-altitude warming
1167 and snow cover retreat over Tibet and the Himalayas enhanced by black carbon aerosols.
1168 Atmospheric Chemistry and Physics 16, 1303-1315.
1169

1170 Zieger, P., Kienast-Sjögren, E., Starace, M., von Bismarck, J., Bukowiecki, N.,
1171 Baltensperger, U., Wienhold, F.G., Peter, T., Ruhtz, T., Collaud Coen, M., Vuilleumier, L.,
1172 Maier, O., Emili, E., Popp, C., Weingartner, E. (2012) Spatial variation of aerosol optical
1173 properties around the high-alpine site Jungfraujoch (3580 m a.s.l.). Atmospheric Chemistry
1174 and Physics 12, 7231-7249.

1175

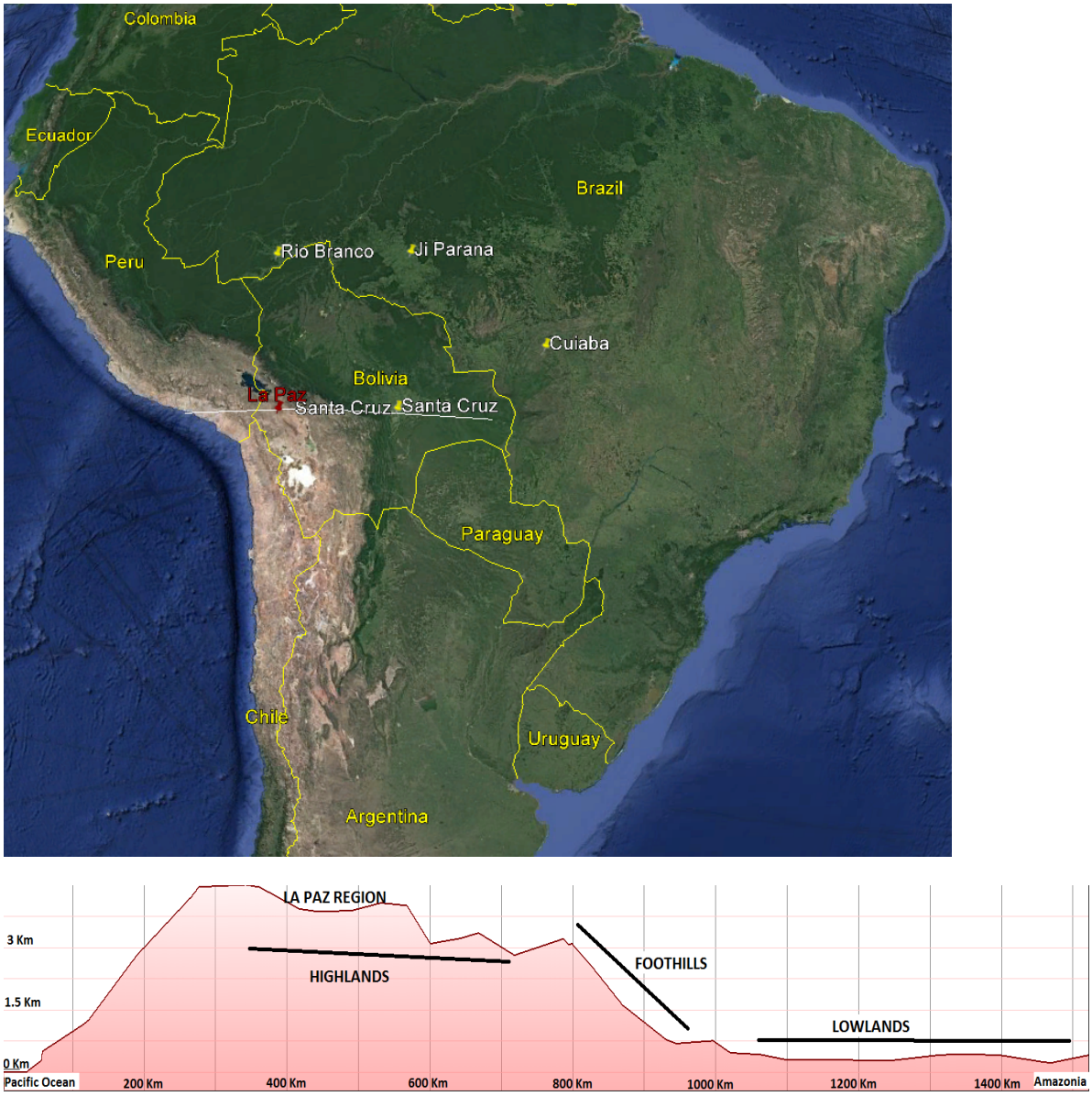

Figure 1: Study region including the AERONET stations used. Horizontal line in the map represents the region of the elevation profile.

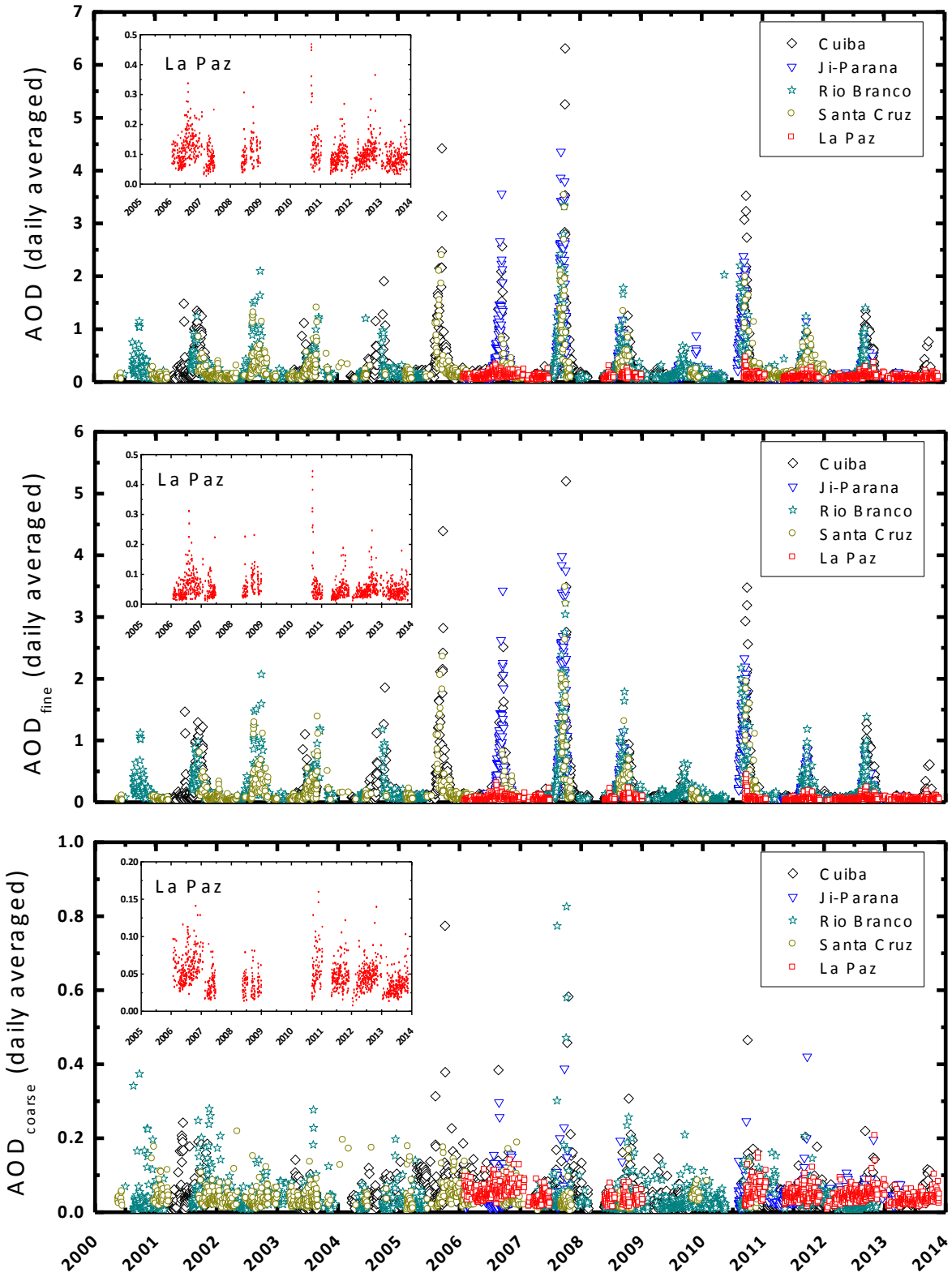

Figure 2: Temporal evolution of daily averaged AOD, including these of the fine and coarse mode. Reference wavelength is 500 nm.

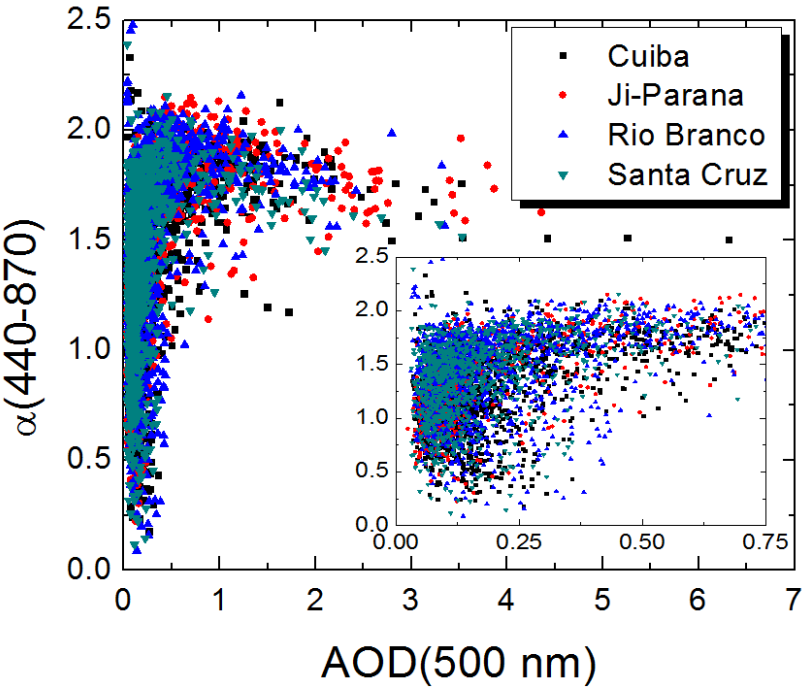

Figure 3: Angstrom exponent versus AOD for the measured points of Figure 2.

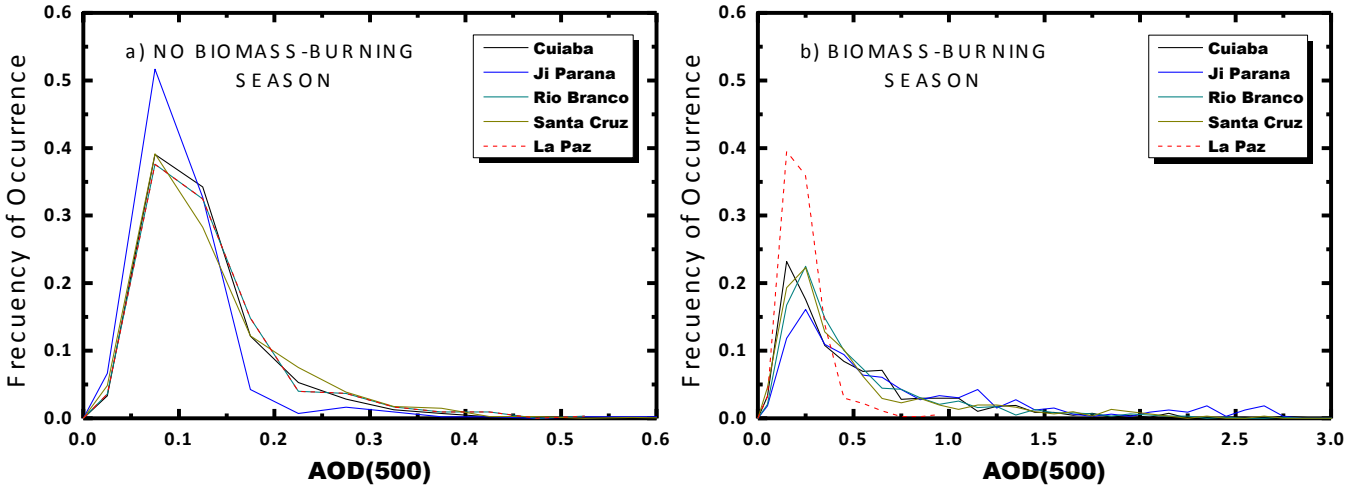

Figure 4: Frequency histograms of aerosol optical depth at 500 nm (AOD(500)) for (a) no biomass-burning and (b) biomass-burning seasons.

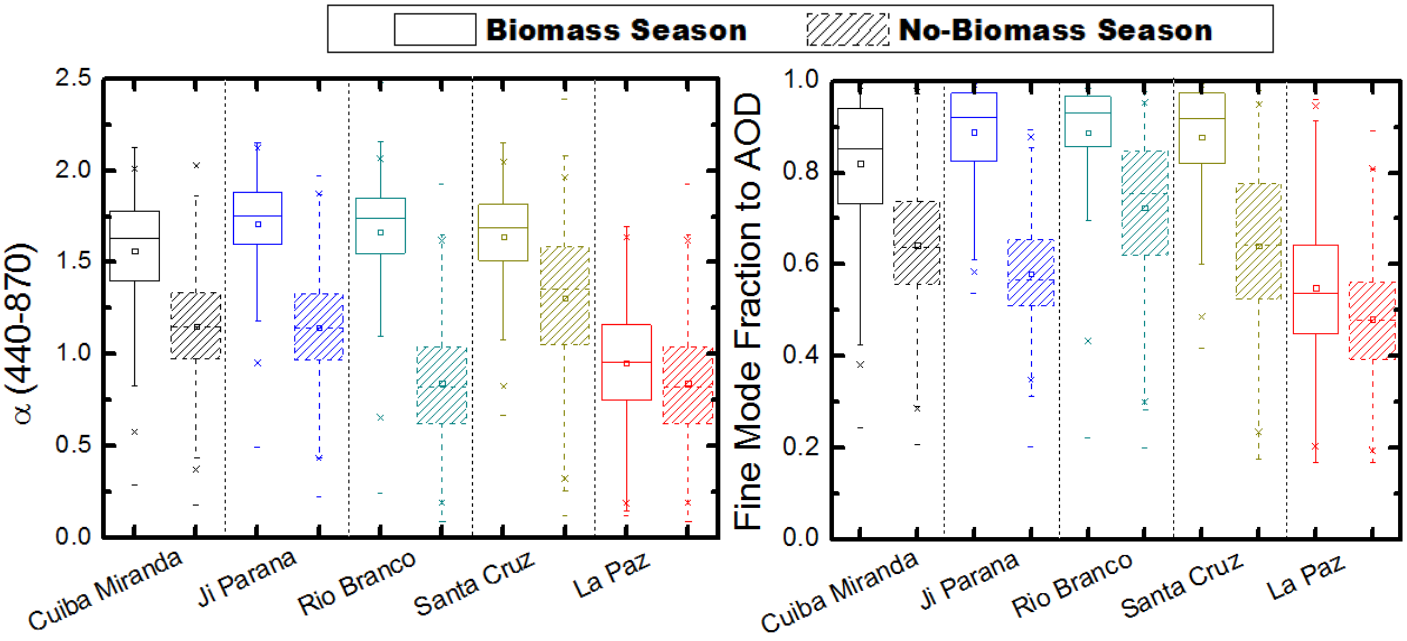

Figure 5: Box-Whisker plots during the biomass and no biomass-burning seasons of the Angstrom parameter α(440-870) and fine mode for the lowlands stations (Cuiaba Miranda, Ji Parana, Rio Branco and Santa Cruz) and highlands station (La Paz). In the Box-Whisker plots, the mean is represented by a very small open square within a given rectangle. The horizontal line segment in the rectangle is the median. The top limit (top of the rectangle) represents the 75th percentile (*P75*) and the bottom limit the 25th percentile (*P25*). The lines perpendicular to the boxes are the 1st (*P1*) and 99th (*P99*) percentiles, and the crosses represent the maximum and minimum values respectively.

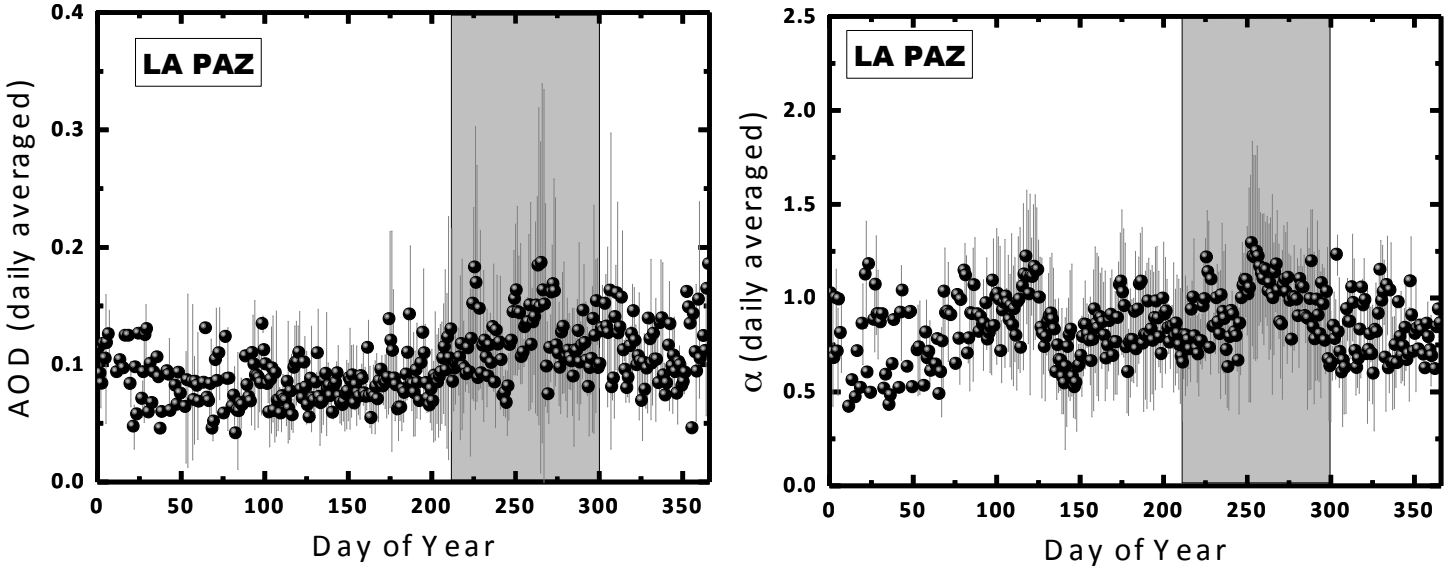

Figure 6: Mean AOD and Angstrom parameter (α(440-870)) , including standard deviations, for every day of the year for the highland station of La Paz. The areas shadowed in light grey represent the biomass-burning seasons.

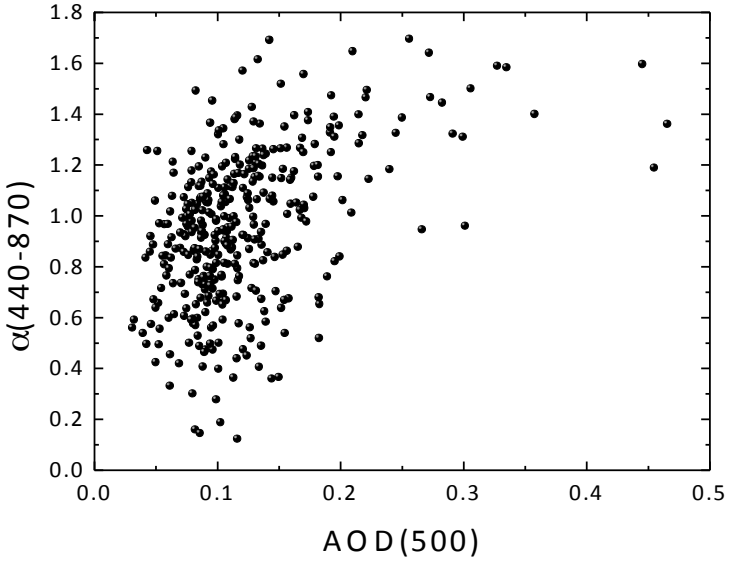

Figure 7: Angstrom exponent versus AOD in the highlands station of La Paz.

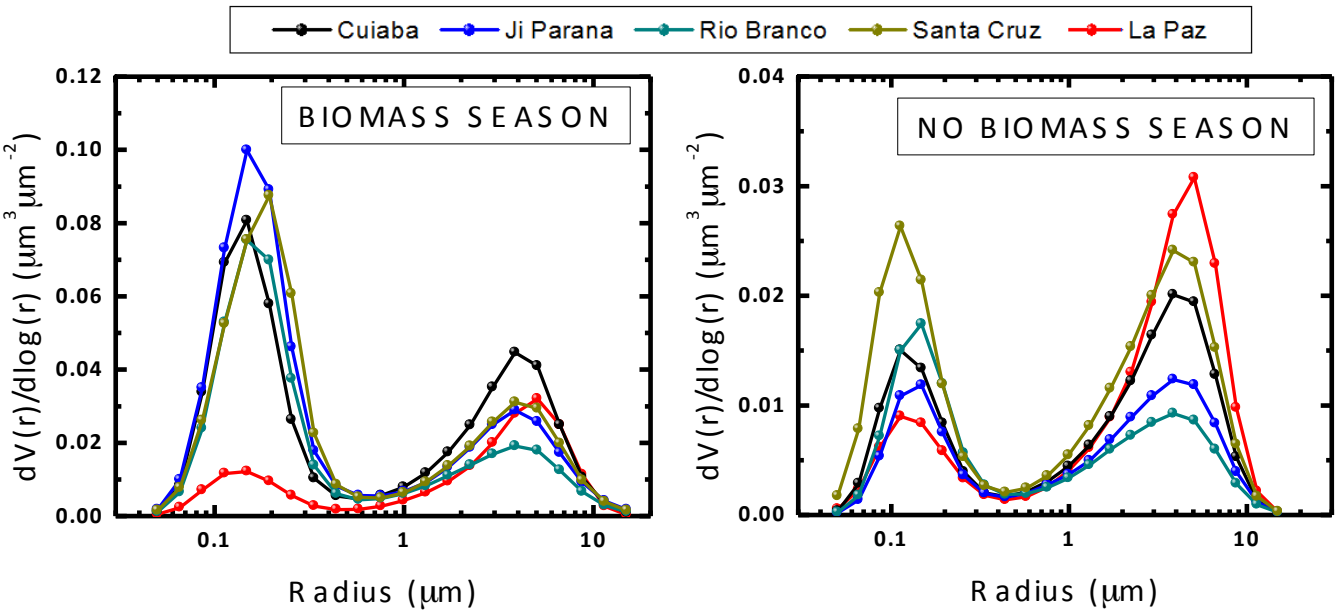

Figure 8: Mean columnar volume size distributions for the lowland stations and highland (La Paz), both for biomass and no biomass-burning seasons.

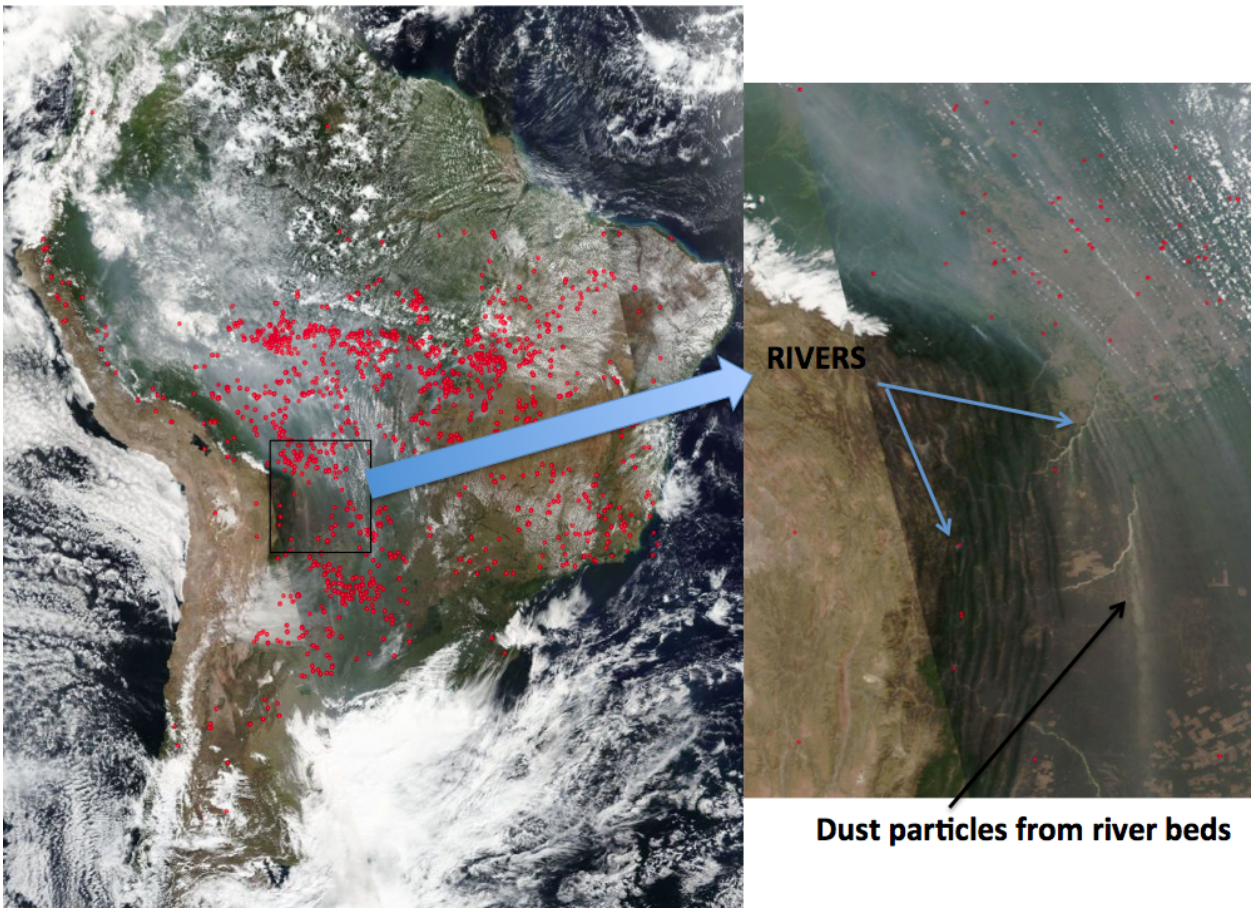

Figure 9: True color image of South America from the composition of images from MODIS (Aqua and Terra) and VIIRS space-systems for 12th September 2016. A zoom is made on the lowlands in Bolivia.

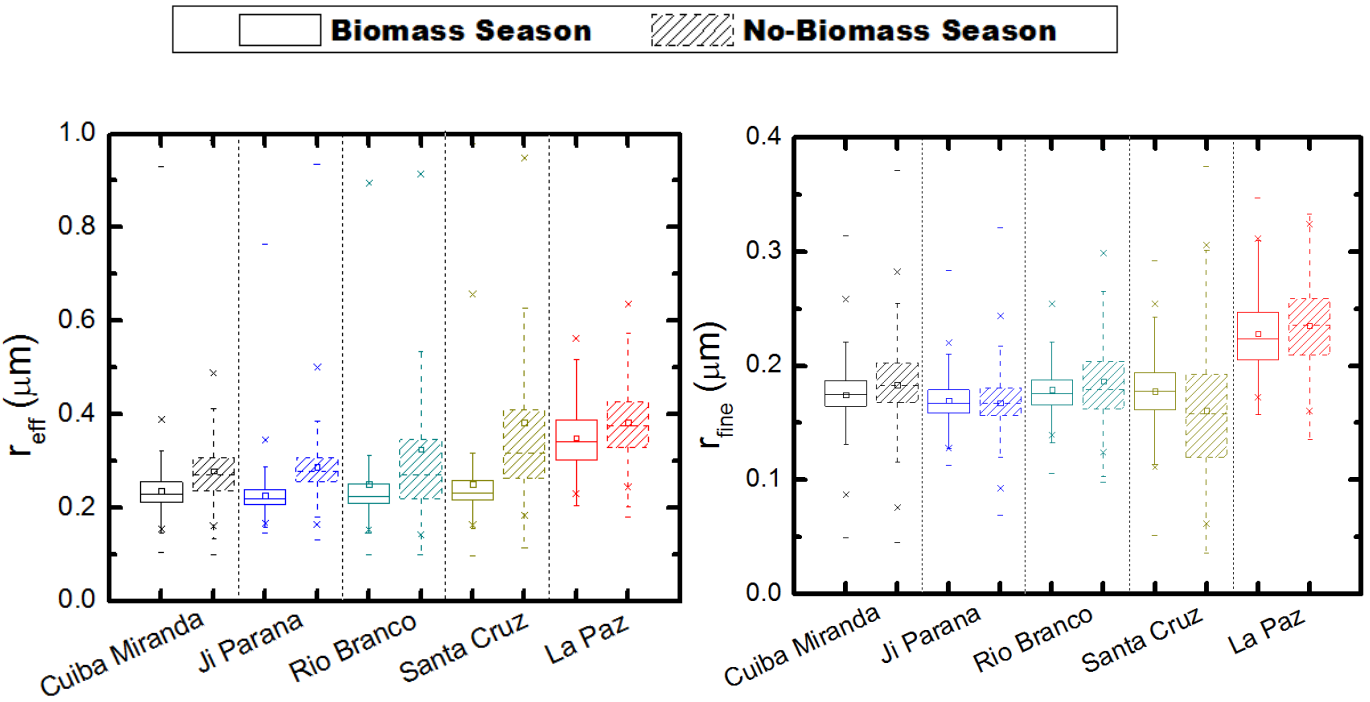

Figure 10: Box-Whisker plots during the biomass and no biomass-burning seasons of the effective radius (r_{eff}) and fine mode effective radius (r_{fine}) for the lowland stations (Cuiaba Miranda, Ji Parana, Rio Branco and Santa Cruz) and the highland station (La Paz). In the Box-Whisker plots, the mean is represented by a very small open square within a given rectangle. The horizontal line segment in the rectangle is the median. The top limit (top of the rectangle) represents the 75th percentile (*P75*) and the bottom limit the 25th percentile (*P25*). The lines perpendicular to the boxes are the 1st (*P1*) and 99th (*P99*) percentiles, and the crosses represent the maximum and minimum values respectively.

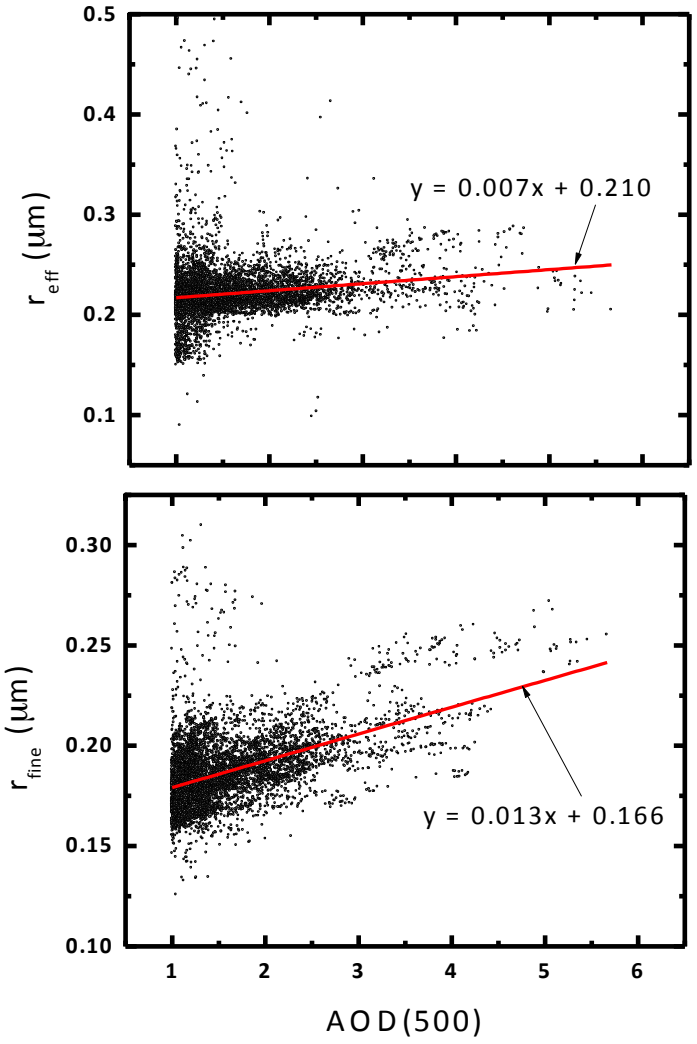

Figure 11: Effective radius (r_{eff}) and effective radius of the fine mode (r_{fine}) versus aerosol optical depth (AOD) at 500 nm for the lowland data. Data selected are for AOD > 1.0.

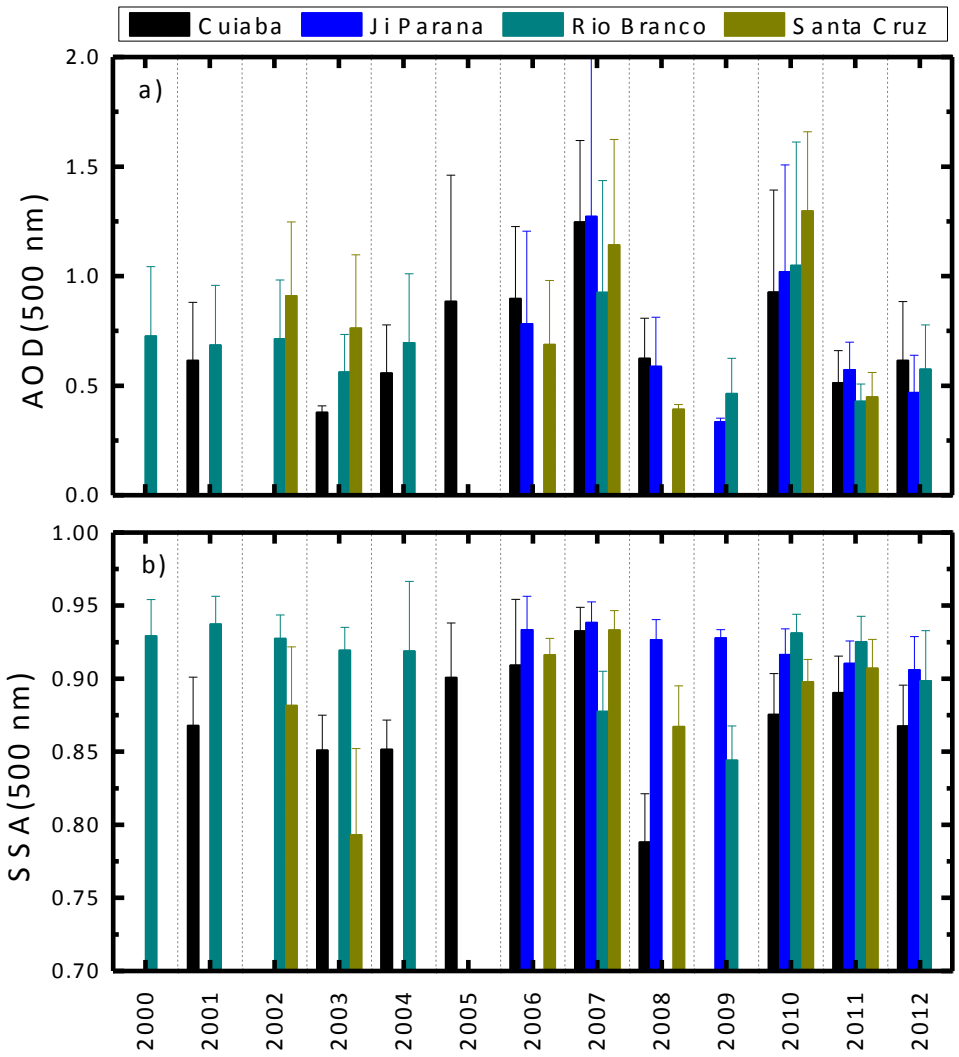

Figure 12: Temporal evolution of the means and standard deviations of (a) aerosol optical depth (AOD) and (b) single scattering albedos (SSA) during the biomass-burning seasons for the lowland. Reference wavelength is at 500 nm.

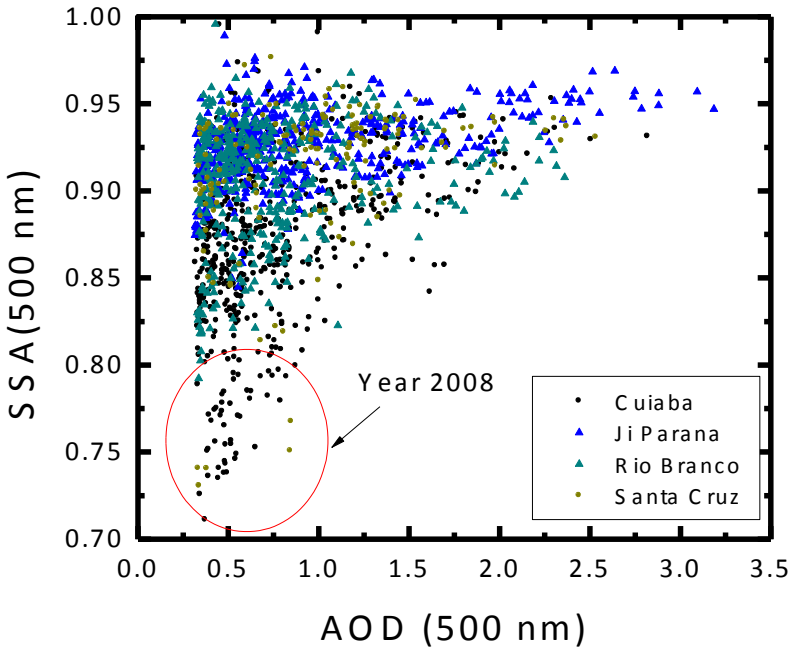

Figure 13: Single scattering albedo (SSA) versus aerosol optical depth (AOD) for the complete AERONET level 2.0 database in the lowlands.

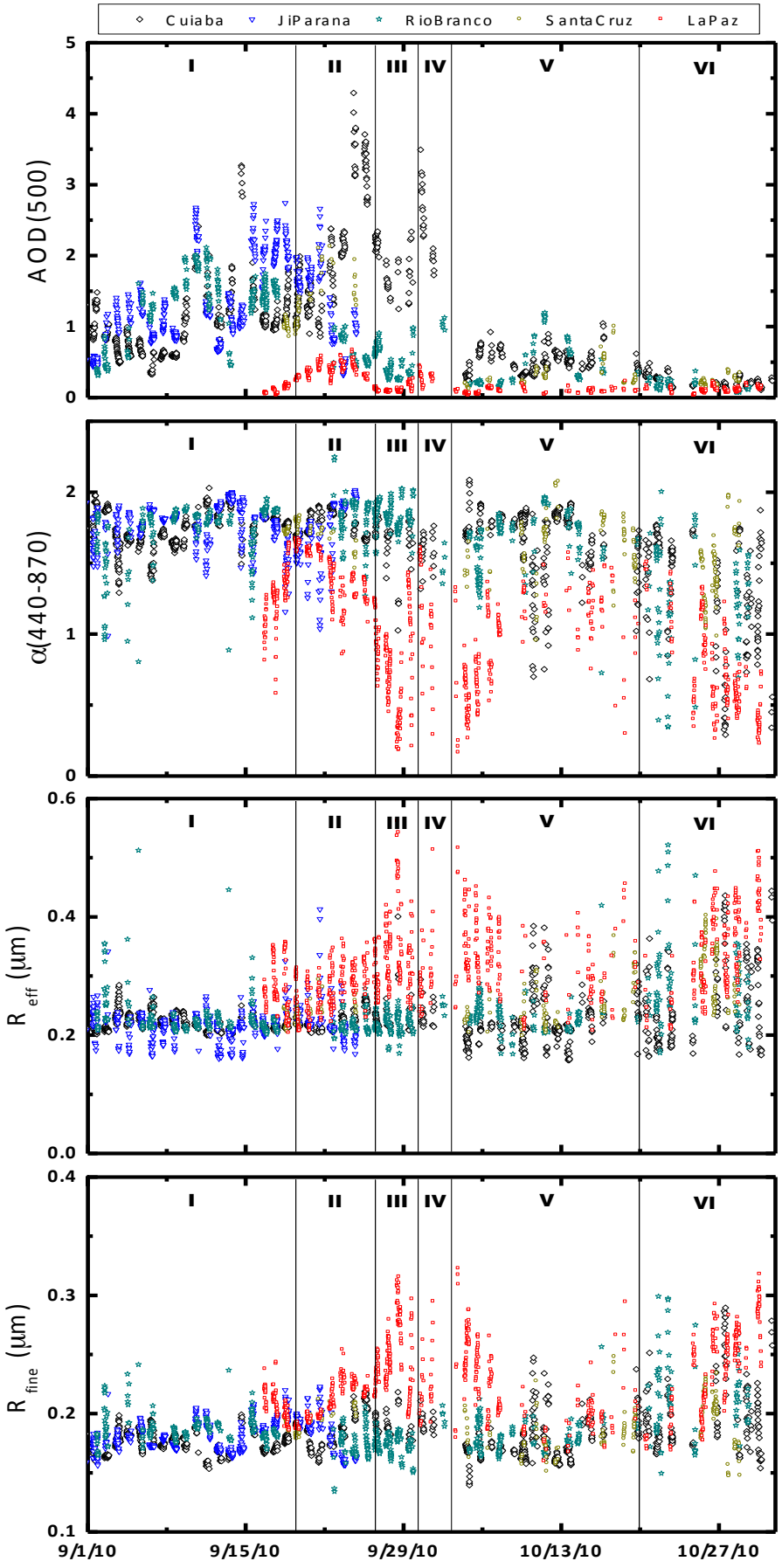
Cuiaba
JiParana
RioBranco
SantaCruz
LaPaz
I
II
III
IV
V
VI
AOD(500)
α(440-870)
R eff (µm)
R fine (µm)
9/1/10
9/15/10
9/29/10
10/13/10
10/27/10

Figure 14: Temporal evolution of aerosol optical at 500 nm (AOD), Angstrom parameter (α(440-870)), effective radius (r_{eff}) and effective radius of the fine mode (r_{fine}) for the period August-October 2010.

a) 2010-09-17 14.55 b) 2010-09-21 14.30 c) 2010-09-26 14.50

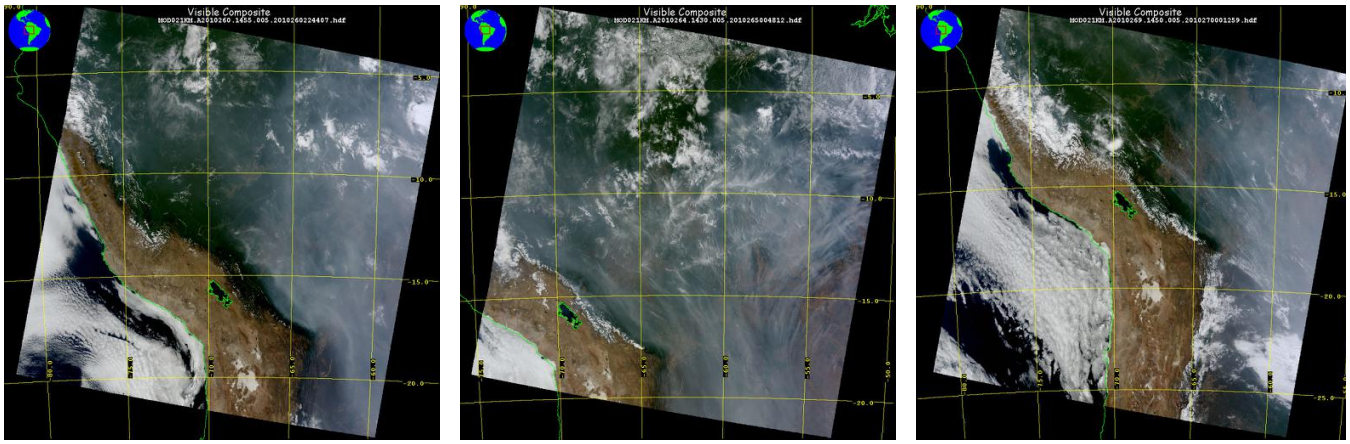

d) 2010-10-03 14.55 e) 2010-10-05 14.45 f) 2010-10-13 18.20

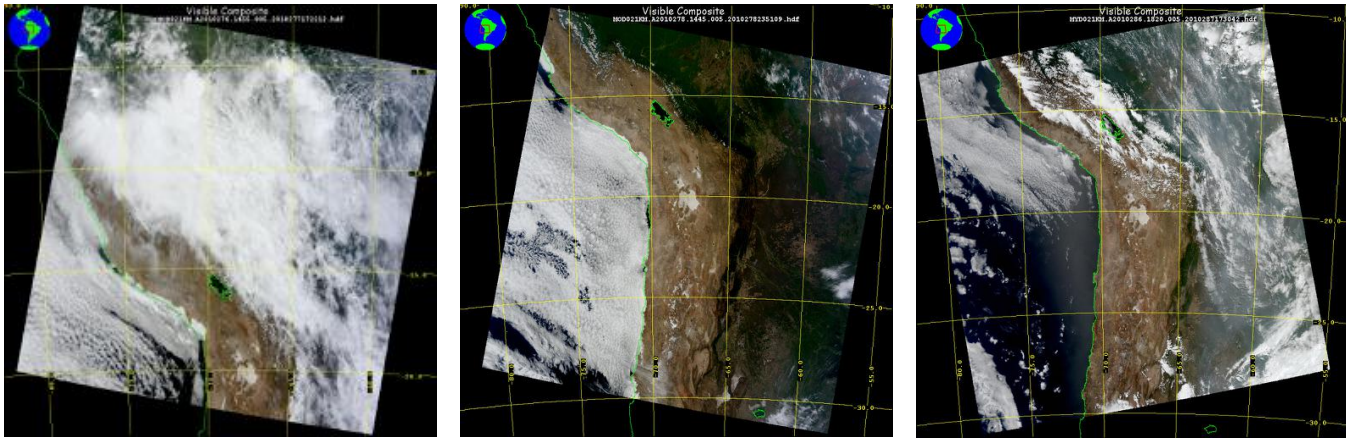

Figure 15: MODIS images for (a) 17/09/2010 (b) 21/09/2010 (c)26/09/2010 (d) 03/10/2010 (e) 05/10/2010 and (f) 13/10/2010

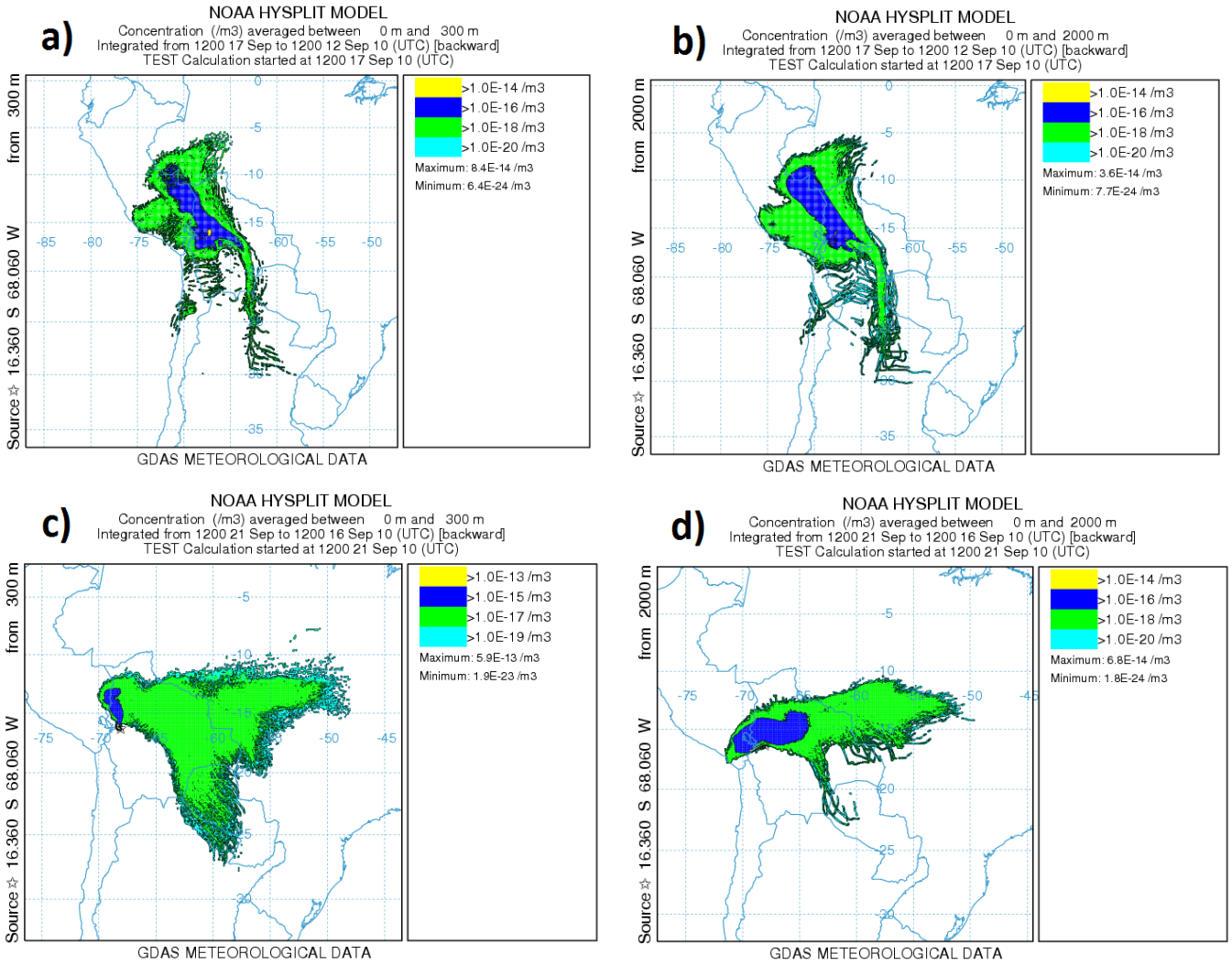

Figure 16: Air concentration backward dispersion for the city of La Paz for 17/09/2010 and 21/09/2010 for two altitude intervals: 0 to 300 m a.g.l. (left hand plots) and 0 to 2000 m a.g.l. (right hand plots). La Paz is identified by the tiny black empty star.

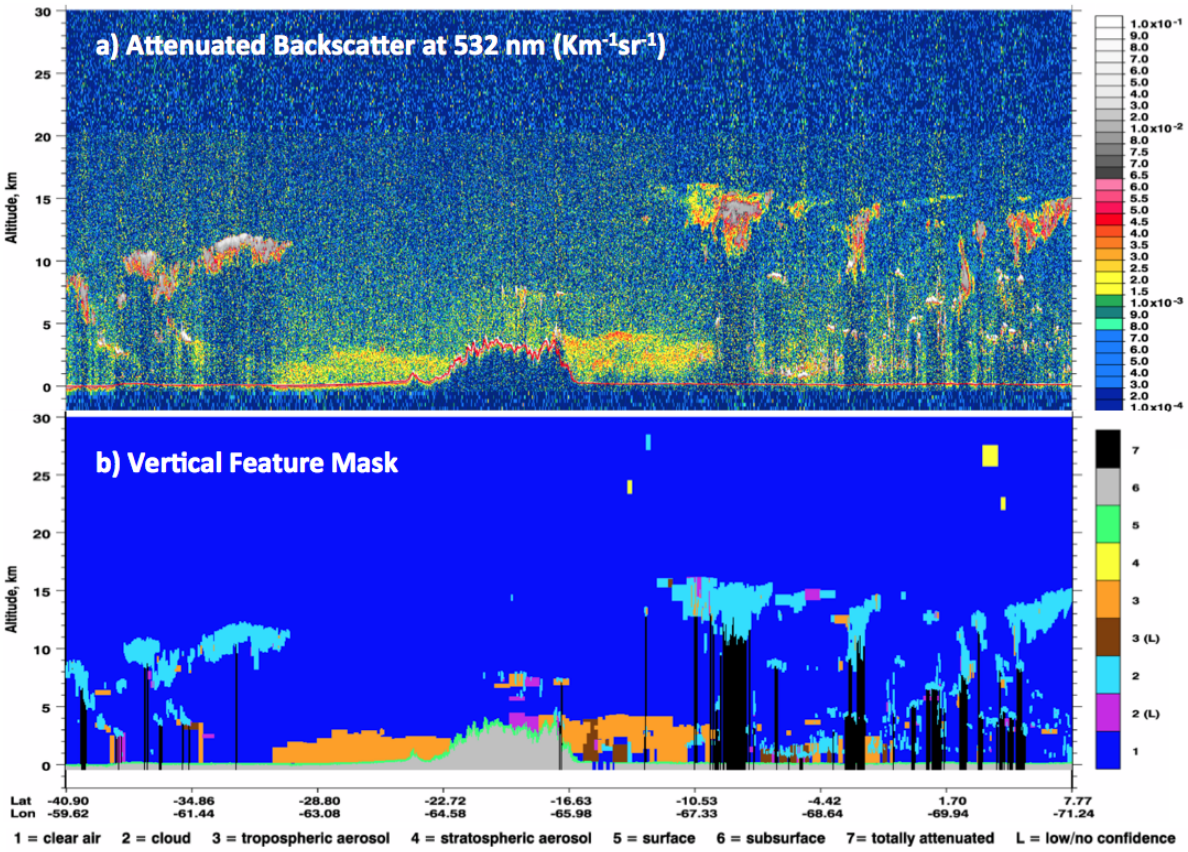

Figure 17: Attenuated backscatter and vertical feature mask for CALIPSO data acquired on 20th September 2010 over South America. Data were acquired between 18:11:49 and 18:25:18 UTC.

		AOD	Alpha	AOD_{fine}	AOD_{coarse}	Eta	AOD	Alpha	AOD_{fine}	AOD_{coarse}	Eta
		Biomas-Burning Season					No Biomass-Burning Season				
Cuiaba	Mean	0.55	1.56	0.48	0.06	0.82	0.13	1.15	0.08	0.04	0.64
	STD	0.61	0.30	0.55	0.06	0.14	0.09	0.32	0.08	0.03	0.14
	Median	0.35	1.63	0.29	0.05	0.85	0.11	1.15	0.07	0.04	0.64
	Max.	6.31	2.12	5.20	0.77	0.99	0.21	2.15	0.19	0.24	0.99
	Min.	0.07	1.41	0.03	0.00	0.24	0.03	0.95	0.01	0.00	0.54
Ji Parana	Mean	0.89	1.71	0.80	0.05	0.89	0.13	1.15	0.06	0.04	0.58
	STD	0.79	0.25	0.79	0.05	0.12	0.09	0.29	0.04	0.02	0.11
	Median	0.50	1.75	0.50	0.04	0.93	0.11	1.14	0.05	0.04	0.57
	Max.	4.36	2.15	3.99	0.42	0.99	0.24	1.97	0.20	0.16	0.89
	Min.	0.07	1.55	0.04	0.01	0.54	0.03	0.95	0.01	0.01	0.20
Rio Branco	Mean	0.52	1.67	0.47	0.04	0.89	0.11	0.84	0.09	0.04	0.72
	STD	0.46	0.29	0.45	0.07	0.12	0.08	0.31	0.06	0.03	0.15
	Median	0.36	1.74	0.31	0.02	0.93	0.09	0.82	0.08	0.02	0.75
	Max.	3.53	2.40	3.22	0.92	0.99	0.19	1.92	0.15	0.18	0.98
	Min.	0.06	1.54	0.04	0.01	0.22	0.02	0.62	0.02	0.00	0.20
Santa Cruz	Mean	0.52	1.64	0.53	0.04	0.87	0.13	1.31	0.09	0.05	0.64
	STD	0.53	0.25	0.57	0.03	0.12	0.09	0.37	0.09	0.02	0.16
	Median	0.33	1.69	0.29	0.03	0.92	0.11	1.36	0.06	0.03	0.64
	Max.	3.53	2.15	3.48	0.17	0.99	0.24	2.4	0.20	0.21	0.98
	Min.	0.06	1.49	0.05	0.00	0.18	0.03	1.05	0.01	0.01	0.17
La Paz	Mean	0.12	0.95	0.07	0.05	0.55	0.09	0.84	0.04	0.04	0.48
	STD	0.06	0.30	0.06	0.02	0.15	0.04	0.31	0.03	0.02	0.13
	Median	0.11	0.95	0.05	0.05	0.53	0.08	0.82	0.04	0.04	0.48
	Max.	0.46	1.69	0.44	0.13	0.95	0.16	1.92	0.14	0.08	0.89
	Min.	0.03	0.74	0.01	0.01	0.17	0.02	0.62	0.01	0.01	0.17

Table 1: Mean, standard deviation (STD), median and maximum (Max.) and minimum (Min.) values of aerosol optical depth (AOD), Angstrom parameter (α) between 440 and 870 nm, fine (AOD_{fine}) and coarse(AOD_{coarse}) mode aerosol optical depths and relative contribution of fine mode to total optical depth (η). Data are presented for biomass and non biomass-burning seasons for the stations in the lowlands (Cuiaba, Ji Parana, Rio Branco and Santa Cruz) and in the highlands (La Paz). Reference wavelength for AOD, AOD_{fine}, $AOD_{coarse}$and η is 500 nm.

	Rainfall Anomaly (mm) for different seasons			Mean AERONET AOD during Biomass-Burning Season
	Wet (199.70 mm)	**Dry (42.97 mm)**	**Biomass-Burning (67.16 mm)**	
2000	2.74	-3.64	-2.06	0.39 ± 0.29
2001	-9.46	3.56	4.74	0.47 ± 0.30
2002	-16.16	1.91	-5.02	0.49 ± 0.37
2003	-20.75	2.81	12.32	0.42 ± 0.27
2004	-2.97	-4.99	-4.35	0.44 ± 0.38
2005	12.08	-4.05	5.28	0.80 ± 0.70
2006	1.69	-9.01	0.72	0.62 ± 0.59
2007	35.70	-12.51	-6.5	1.18 ± 1.00
2008	9.20	-12.07	-1.30	0.43 ± 0.29
2009	10.02	7.27	0.17	0.20 ± 0.11
2010	3.41	-11.91	-5.91	0.95 ± 0.67
2011	5.77	-11.57	-6.70	0.32 ± 0.21
2012	-13.08	7.28	-12.94	0.40 ± 0.27
2013	41.18	9.13	15.94	0.29 ± 0.19

Table 2: Precipitation anomaly for 'wet' (November-March), 'dry' (April-July) and biomass-burning seasons (August-October). The mean climatological values are in parentheses. The anomaly is defined as the difference between registered and climatological values for each season. All precipitation data were acquired by the TRMM satellite and are the average over the area 10-20 South and 50-70 West. The AOD column is the average, at 500 nm, across the biomass burning season for the lowland stations at Cuiaba, Ji Parana, Rio Branco and Santa Cruz. The "Wet" column represents data whose November to March period started in the previous year

		r_{eff}	rf_{ine}	r_{eff}	rf_{ine}
		Biomas-Burning		**No Biomass**	
Cuiaba	Mean	0.24	0.18	0.27	0.20
	STD	0.05	0.03	0.07	0.04
	Median	0.23	0.18	0.27	0.20
	Max.	0.93	0.31	0.99	0.38
Ji Parana	Mean	0.22	0.17	0.29	0.16
	STD	0.03	0.02	0.06	0.05
	Median	0.22	0.17	0.28	0.17
	Max.	0.76	0.28	0.93	0.35
Rio Branco	Mean	0.25	0.18	0.32	0.19
	STD	0.11	0.02	0.18	0.03
	Median	0.22	0.17	0.27	0.18
	Max.	1.05	0.32	1.01	0.38
Santa Cruz	Mean	0.25	0.18	0.38	0.13
	STD	0.08	0.03	0.19	0.06
	Median	0.23	0.17	0.31	0.12
	Max.	0.97	0.28	1.17	0.39
La Paz	Mean	0.34	0.22	0.38	0.24
	STD	0.07	0.03	0.08	0.04
	Median	0.34	0.16	0.37	0.23
	Max.	1.14	0.35	1.08	0.51

Table 3: Mean, standard deviation (STD), median and maximum (Max.) values of effective radius (r_{eff}) and effective radius of the fine mode (r_{fine}). Data are presented for biomass and no biomass-burning seasons for the lowland stations (Cuiaba, Ji Parana, Rio Branco and Santa Cruz) and the highlands (La Paz).

		SSA	g	m_r	m_i
Cuiaba <554>	Mean	0.88	0.65	1.46	0.019
	STD	0.05	0.02	0.06	0.010
	Median	0.88	0.65	1.47	0.017
	Max.	1.00	0.72	1.6	0.060
	Min.	0.71	0.59	1.34	0.001
Ji Parana <492>	Mean	0.92	0.65	1.48	0.011
	STD	0.02	0.02	0.05	0.004
	Median	0.93	0.65	1.48	0.011
	Max.	0.99	0.73	1.60	0.027
	Min.	0.84	0.59	1.34	0.001
Rio Branco <425>	Mean	0.91	0.66	1.47	0.015
	STD	0.04	0.02	0.05	0.007
	Median	0.92	0.73	1.47	0.013
	Max.	1.00	0.66	1.60	0.044
	Min.	0.79	0.60	1.34	0.001
Santa Cruz <158>	Mean	0.91	0.67	1.48	0.015
	STD	0.04	0.02	0.05	0.010
	Median	0.93	0.67	1.48	0.011
	Max.	0.98	0.71	1.60	0.065
	Min.	0.73	0.61	1.34	0.003
La Paz <36>	Mean	0.87	0.68	1.50	0.016
	STD	0.04	0.02	0.07	0.007
	Median	0.87	0.69	1.50	0.015
	Max.	0.93	0.72	1.60	0.036
	Min.	0.78	0.61	1.35	0.007

Table 4: Mean, standard deviation (STD), median and maximum (Max.) and minimum (Min.) values of aerosol single scattering albedo (SSA), asymmetry factor (g) and real (m_r) and imaginary (m_i) part of refractive index. Data are presented only for biomass-burning data as most of the data that fulfill AERONET requirements are acquired in this season. These values are the result of linearly interpolating retrieval values at 440-670 to 500 nm. Data in brackets represent the number of retrievals for each place.